System Modeling of Next Generation Digitally Modulated Automotive RADAR (DMR)

by

Prassana Kalyan

A Thesis Presented in Partial Fulfillment
of the Requirements for the Degree
Master of Science

Approved July 2019 by the
Graduate Supervisory Committee:

Bertan Bakkaloglu, Co-Chair
Jennifer Kitchen, Co-Chair
Douglas Garrity

ARIZONA STATE UNIVERSITY

August 2019

ABSTRACT

State-of-the-art automotive radars use multi-chip Frequency Modulated Continuous Wave (FMCW) radars to sense the environment around the car. FMCW radars are prone to interference as they operate over a narrow baseband bandwidth and use similar radio frequency (RF) chirps among them. Phase Modulated Continuous Wave radars (PMCW) are robust and insensitive to interference as they transmit signals over a wider bandwidth using spread spectrum technique. As more and more cars are equipped with FMCW radars illuminate the same environment, interference would soon become a serious issue. PMCW radars can be an effective solution to interference in the noisy FMCW radar environment. PMCW radars can be implemented in silicon as System-on-a-chip (SoC), suitable for Multiple-Input-Multiple-Output (MIMO) implementation and is highly programmable. PMCW radars do not require highly linear high frequency chirping oscillators thus reducing the size of the final solution.

This thesis aims to present a behavior model for this promising Digitally modulated radar (DMR) transceiver in Simulink/Matlab. The goal of this work is to create a model for the electronic system level framework that simulates the entire system with non-idealities. This model includes a Top Down Design methodology to understand the requirements of the individual modules' performance and thus derive the specifications for implementing the real chip. Back annotation of the actual electrical modules' performance to the model closes the design process loop. Using Simulink's toolboxes, a passband and equivalent baseband model of the system is built for the transceiver with non-idealities of the components built in along with signal processing routines in Matlab. This model provides a platform for system evaluation and simulation for various system scenarios and use-cases of sensing using the environment around a moving car.

DEDICATION

To the memory of my loving parents,

Rajeswari

&

Kalyanasundaram

ACKNOWLEDGMENTS

I sincerely thank my Professors Dr Bertan Bakkaloglu, Dr Jennifer Kitchen and Dr Douglas Garrity for providing me this opportunity to work with them and pursue this research. I am forever in their debt for the learning and understanding derived from their lectures and this work. I thank NSF and NXP for funding this work and helping to further it with an internship.

I thank my wife Srinandhini for supporting me to pursue my dream of graduate school and standing by me through the thick and thin of times. I thank our lovely little daughter Raji for bringing a smile upon my face every single time that I see her.

I deep heartedly thank all my friends who has supported me throughout my life and the new friends that I have made here during my classes and in my tenure at the Power One Lab. I thank ASU's school of Electrical Computer and Energy Engineering for the providing me this opportunity to learn and advance my career.

TABLE OF CONTENTS

Page

CHAPTER Page

LIST OF TABLES

LIST OF FIGURES

Figure Page

CHAPTER 1

INTRODUCTION

Radio **D**etection **A**nd **R**anging (RADAR) systems are useful electronic systems whose valuable service in the World War II helped the allies win the war and began an era of electronic intelligence in warfare. Though radars reached their prominence only during the war, the idea was conceived as early as 1903 by Christian Hülsmeyer to avoid collision of ships when docking at the harbor at night or under a thick fog [1]. After the success of war, radars were an area of active research and deployed in many applications - civilian aviation, aerial and maritime navigation, geo-mapping, meteorology, radio astronomy and remote sensing.

A radar sensor illuminates the environment around using radio waves, like a searchlight, and tunes to receive the reflected faint radio waves to estimate the distance, velocity and size of the target. The radio waves are also reflected from the surrounding environment that represent the clutter in the observed signal. A radar is expected to discard clutter and represent the target amidst its own system noise. A radar system can operate in two different modes, only transmit or receive at a given time (monostatic) or transmit and receive at the same time (bistatic).

1.1 RADAR for Advanced Driver Assistance Systems

Luxury cars since the late 1990's include some form of Driver Assistance Systems [50][51][52]. The current Advanced Driver Assistance Systems (ADAS) includes a host of functions that perform Adaptive Cruise control, Collision warning, Collision Mitigation, Lane Departure warning, Traffic sign recognition, Backup Autonomous driving, Lane assist, Blind spot detection, Backup and Park Assist, Driver attention, gesture recognition, High Beam Assist etc. to ensure safety of the commuters. ADAS relies on an

array of heterogenous sensors which include camera, Light Detection And Ranging (LIDAR) sensors, ultrasonic sensors and automotive radars (autoradars). The frequency of operation of the latest and upcoming radars technologies work on newly allocated 76-81 GHz range which enable accurate detection of targets due to their shorter wavelengths [11],[25]. Realizing these radar systems usually includes a multi-chip solution that increases cost and demands larger housing and cooling arrangement and hence are suitable to the luxury segment.

Radars for automotive applications were tested from the early 1970s [12] and were installed as standalone systems with cars. The increased awareness among people to make roads safer is pushing autoradars' adoption on a larger scale. Autoradars are classified into three major classes based on their end range and range resolution [11]. A typical ADAS car with different radars and their ranges [13] is shown here.

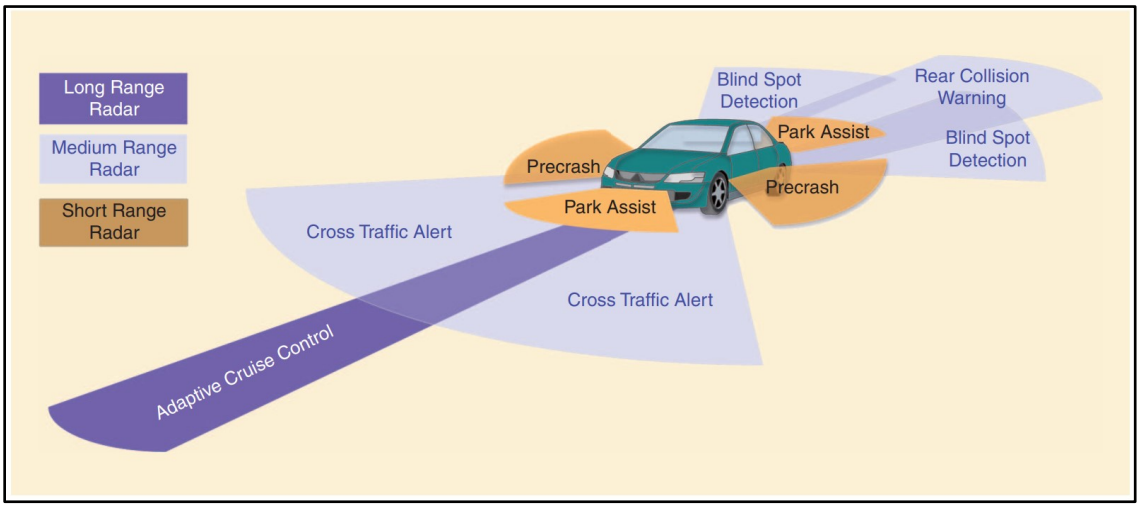

Figure 1: Automotive Radar Types [13]

The following table shows the specifications for the three different autoradars and their application.

Type	Long Range Radar	Medium Range Radar	Short range radar
Max power (EIRP)	55 dBm	-9 dBm/MHz	-9 dBm/MHz
Frequency band	76 – 77 GHz	77 – 81 GHz	77 - 81 GHz
Bandwidth	600 MHz	600 MHz	4 GHz
$R_{min} - R_{max}$	10 – 250 m	1 – 100 m	0.15 – 30m
Range resolution	0.5m	0.5m	0.1m
Range accuracy	0.1m	0.1m	0.02m
Velocity resolution	0.6 m/s	0.6 m/s	0.6 m/s
Velocity accuracy	0.1 m/s	0.1 m/s	0.1 m/s
Angular accuracy	0.1^{o}	0.5^{o}	1^{o}
Applications	Adaptive cruise control	Lane-change assist, cross-traffic alert, blind-spot detection, rear-collision warning	Park assist, obstacle detection, pre-crash

Table 1: Automotive Radar Specifications and Classifications

1.2 Motivation

The autoradars deployed in cars are expensive as these systems use several integrated circuits (ICs) to realize the system. These also include specialized Silicon-Germanium (SiGe) process which has higher cost per transistor rather than the Complementary Metal Oxide Semiconductor (CMOS) technology. CMOS allows extremely low power, low

cost per transistor and high integration ability. The state-of-the-art radar technology uses a linear Frequency modulation pulse compression method commonly known as Frequency Modulated Continuous Wave (FMCW) radars. The performance of these radars is, however, poor in a dense environment crowded with other radars [20]. Avoiding interference in a multi radar environment and is an area of active research [44][45][46] for FMCW radars.

Phase modulated continuous wave radars (PMCW) provide an excellent alternative to FMCW radars and are used in military and can be used in a radar noisy environment due to the merits of spread spectrum technique. PMCW radars are only in evaluation phase [39] for automotive radars and provides a great avenue for research and development.

Top down design methodology has advantages of being able to make significant design decisions very early in the design process. Behavioral modeling of systems provides a platform to build the system and simulate for different test conditions to understand the validity of the system specifications for the end application. Simulink/Matlab is a well-known mathematical modeling tool for modeling and simulation as it includes many industry standard functions and toolboxes.

The aim of this thesis is to understand the system requirements and develop a PMCW radar model that is capable of being programmed for different applications. Many prebuilt Matlab/Simulink models are available to demonstrate FMCW radar's working, no such models are available for PMCW. This work aims to create a PMCW radar transceiver model with non-idealities and backend signal processing. As the approach is to build an interference robust radar, it is required by design, to have maximum programmability for this autoradar to make it appear unique among other radars. Such a programmable PMCW radar system is hereby referred as Digitally

Modulated Radar (DMR) as the radar signal is now modulated by a stream of different sets of pseudo random binary digits.

The goal of this project is to provide a platform to derive the electrical module level specifications that are required to meet the performance characteristics of the radar. The model should also be able to back-annotate the specifications from the actual design simulations and predict the performance of the radar.

1.3 Organization of the Thesis

The thesis is organized as follows:

Chapter 2 discusses the theory of operation of Radars, trends in radars and the choice of radar for this thesis. It also introduces to the fundamentals of signal processing of DMRs.

Chapter 3 discusses the System Model development using Simulink/Matlab and discusses the methods of implementation of Transceiver and the signal processing algorithms.

Chapter 4 discusses the results of the model and results of various system scenarios simulated. It also presents a discussion about the optimal performance specifications for the system.

Chapter 5 discusses future work in the direction of using this DMR model to explore various architectures for implementing with different integration technologies.

CHAPTER 2

BACKGROUND

2.1 Continuous Wave Radars for Automotive Applications

Continuous Wave (CW) Radars used in Doppler Radars for motion sensing emits a continuous high frequency carrier signal towards the target. As the target's velocity changes, wavelength of the reflected signal changes due to doppler effect. The beat frequency between the transmit and the received radar signals represents velocity of the target. Thus, Doppler radars are used in Traffic control and motion monitoring applications use a continuous wave instead of pulsed operation. CW radars require a bistatic arrangement to use separate transmit and receive antennas as they are work simultaneously.

Though CW radars can measure the velocity of the target due to the doppler shift of the carrier, it is not possible to measure the range. Traditional (pulsed) radar uses a single narrow pulse aimed at the target and capture the echo to decode the range of the target. Integrated circuits are not suitable for pulsed radar operation due to their limited transmit power and dielectric strength. Pulsed Doppler radars combined the benefits of both conventional pulsed radars and the continuous wave radars to determine range and velocity of targets. However, the range resolving ability of the radar was limited by the continuous wave pulse width.

To overcome the signal shape's dependence on resolution, Pulse Compression is a technique used since early radars. By pulse compression, the radar emits a long pulse that is spectrally similar to a narrow time domain pulse at the receiver. The conversion of wide time pulse to a spectral narrow pulse is achieved by matched filtering, thus exhibiting the same performance of a pulsed radar to measure range. The doppler shift of

the continuous wave can be used to determine the velocity of the target. In practice, to achieve pulse compression and maximum range detection, Continuous Wave Radars with pulse compression are used. A basic autoradar's block diagram is presented below.

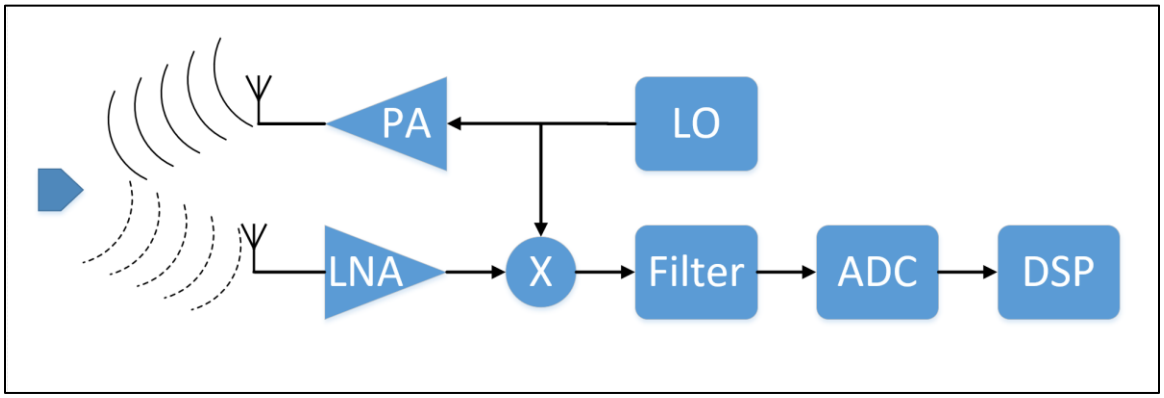

Figure 2: Basic Block Diagram of Modern Bistatic Autoradar

2.2 Pulse Compression

Instead of a pulse of very high power (P_1) with a narrow width (τ_1), pulse compression radars transmit a long pulse with wider pulse width (τ_2) and reduced power (P_2). This can be achieved by modulating the frequency or phase of the carrier. By doing so, the radar bandwidth (B_r) of the transmitted signal is varied to achieve required range resolution as the radar bandwidth is now controlled by the modulating signal's bandwidth (indirectly). This idea is utilized in automotive radars thus paving way for Continuous Wave operation instead of pulsed operation. [4]. Pulse compression can be achieved by the following methods

- Linear Frequency Modulation (LFM) of the carrier,
- Nonlinear Frequency Modulation of the carrier, and
- Phase Modulation of the carrier

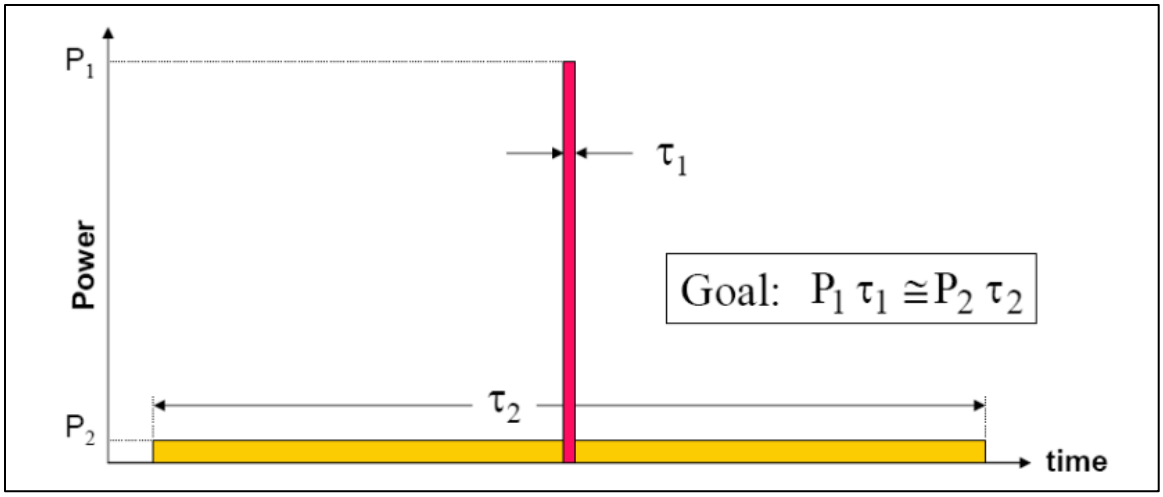

Figure 3: Pulse Compression [18]

Among these techniques of Pulse compression [4], Linear Frequency modulation Continuous Wave Radars (FMCW) are extensively used for Automotive radars. This thesis attempts to provide a model for another type of Pulse compression radar – Phase Modulated Continuous Wave Radar (PMCW) which can be configured for wide radar bandwidth for its advantages over FMCW [15] [16] [23].

2.3 FMCW Radars

Linear FMCW radars were conceived in the early 1930s and still the most popular pulse compression method. FMCW radars transmit a continuous frequency varying RF carrier signal known as a chirp $f_T(t)$. This signal is reflected of the target and picked up by the receiver and mixed with the instantaneous chirp to down convert the signal to 0 Hz. The beat frequency between the received chirp and the instantaneous chirp in the transmitter produces an intermediate frequency is now proportional to the target's distance f_{IF}. The time delay between the transmit and the receive signal indicates twice the distance that the waveform has travelled with the speed of light t_d. Pictorially, this can be represented as below

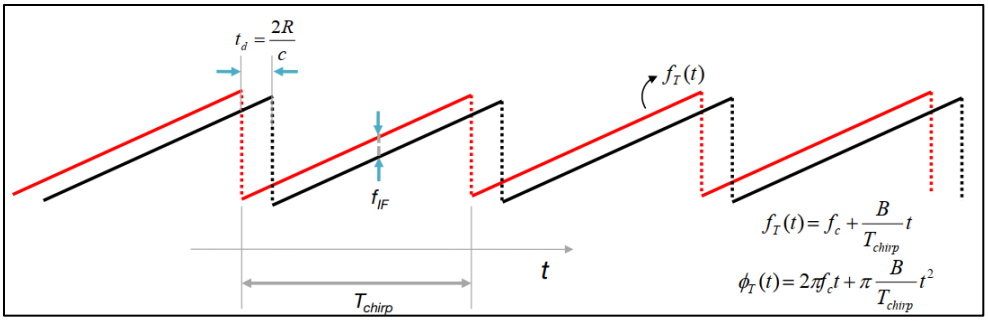

Figure 4: FMCW Radar Operation [28]

The beat frequency (f_{IF}) is limited by the slope of the chirp. This is usually limited to 30 MHz or lower in commercial radars. FMCW radars, thus, requires a very highly linear VCO capable to chirp for different frequency ranges. To satisfy the requirements for SRR and USRR, FMCW radars may be required to be able to sweep the entire autoradar bandwidth of 77-81 GHz in a perfectly linear fashion. This is a tough engineering problem in CMOS.

Though FMCW is advantageous by having a very deterministic waveform [4], it suffers interference due to other FMCW radar s that may operate in the vicinity [20]. The occupied baseband bandwidth of FMCW radars are smaller and thus provide high SNR due to smaller equivalent noise bandwidth (ENBW) in the system. The signal sweep range and baseband bandwidth are not related directly, as FMCW radars can sweep at a different ramp rate. The sweep rate is also limited by the RF VCO's ability to track the control voltage without losing lock while maintaining linearly varying frequency output and fast settling capability [26]. The VCO, by design, only allows only a finite rate of change of frequency, thereby limiting the range of possible beat frequency bandwidth. Since FMCW is a non-coherent radar, the system noise is dominated by the phase noise of the VCO. A wide bandwidth and stable Low phase noise VCO limit the radar for very precise measurements.

Moreover, FMCW radars also need complex floating-point arithmetic digital signal processing. The Digital power consumption can be reduced by pursuing deep submicron transistors and FinFET structures but realizing RF and VCO performance becomes challenging and makes integrating all these subsystems a System-on-Chip (SoC) a daunting task.

2.4 Comparison of FMCW and PMCW Radars

Compared to FMCW radar, PMCW has several important advantages. First, PMCW radars need a constant frequency carrier input. Since PMCW is a coherent radar, if the phase noise of the PLL at 1 MHz offset attains -94 dBc/Hz [16] the phase noise can be ignored as the transmit and receive paths use the same clock for a target at a maximum range of 30 meters. Secondly, the range resolution and the range of the system can be changed by changing the chip's clock frequency.

PMCW radar systems can have zero range sidelobes, if they use PN codes with perfect correlation properties [26]. PMCW systems offer high interference robustness using spread spectrum techniques to strong interferers. They do not require high-speed, fast-settling frequency synthesizers [26]. Finally, the transmitter's phase modulation transceiver can also serve as the same hardware for Inter-vehicular (IVx)/Vehicle to Vehicle communication(V2V) [32].

2.5 Literature Review

With the overwhelming advantages of PMCW radars, the present trends of PMCW radars were studied to analyze their suitability for autoradars. Among them, Jalli Ng's work[15] on patient monitoring system using pseudo-random noise coded Doppler radar transceiver was reviewed. The paper points out the merits of using PMCW based radars for accurate measurement of small targets and changes to environment. Since, DMR is

expected to suit a very wide bandwidth autoradar frequency range, this could be a possible solution. Though, this solution is implemented in a special Silicon-Germanium process, key takeaways from this work were the system realization architecture and the possibility of such a solution.

A brief learning on the chaos-based radars was done to see if it would be feasible for autoradars [47],[48]. This radar works on the principle that a signal based on a nonlinear chaotic map that has an excellent autocorrelation property be used as the radar signal waveform to detect objects. This work also clearly demonstrates the use of a perfect correlating sequence (produces a thumbtack like ambiguity function) can be used to detect objects.

Compressive sensing-based noise radars are attractive solutions for short distances and slow targets, but the sparse signal processing method in the baseband to recover the medium and long-range targets was demonstrated in [56]. But these models had a significantly higher relative errors for the measurements.

The most impressive PMCW radars for automotive applications were created by IMEC [16],[17]. The authors clearly harnessed the power of spread spectrum and multiple-input-multiple-output (MIMO) and high correlation peak sequences. The work is also complete with a SoC manufactured and shared the test results. Though the chip was started for 30m SRR, due to size constraints, were manufactured for only 3m Range and tested only for 1.5m. This work presented an excellent starting point for the idea of DMR as many design details were unclear. Oscar's work [18] presents a lot of details on the signal processing aspects. These works are the starting point for the model that is created here.

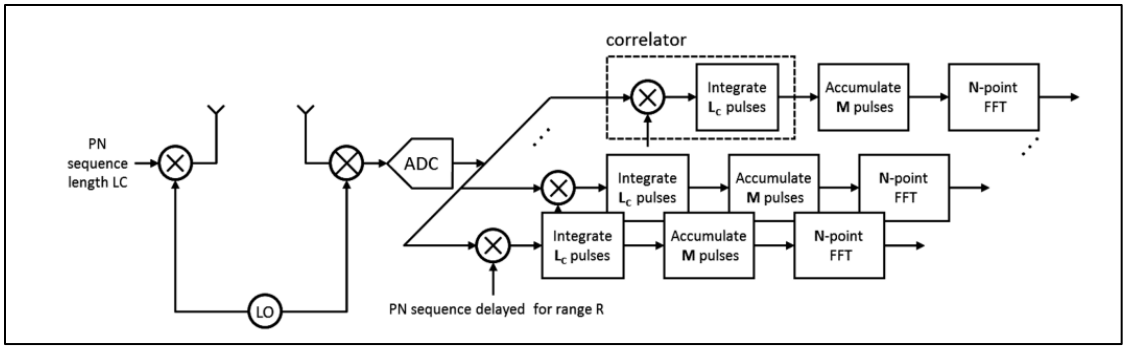

Figure 5: Simplified Block Diagram of PMCW Radar [17]

2.6 Main Concepts of Radar Applicable to DMR

Before we delve into the aspects of DMR, it is worthwhile to learn about the general radar concepts as it would be necessary to build the matlab models.

2.6.1 Radar Equation

The Radar equation presents the relationship between the transmitted power to the received power based on an isotropic antenna gain with a radar cross section RCS **σ** at a distance R from the radar.

$$P_{RX} = \frac{P_{TX} G_{TX} G_{RX} \lambda^2 \sigma}{(4\pi)^3 R^4 L_{TX} L_{RX}}$$

where, P_{RX} – Received signal power,

P_{TX} – Transmitted signal power,

G_{TX},G_{RX} – Isotropic gain of TX and RX antenna,

λ – Carrier signal wavelength,

σ – Radar cross section of the target,

R – Range of the target; and

L_{TX},L_{RX} – Insertion loss of TX and RX antenna

The ability of the radar receiver to detect received signals from the target depends on the radar receiver's sensitivity S_r [2]. Theoretically for conventional pulsed radars, the minimum detectable signal is defined by $S_r$and if received signal power P_{RX} above S_r, the target can be detected. Sensitivity is defined by the Receiver Noise temperature, Noise Equivalent Bandwidth (B_n) of the receiver system and the input referred Signal-to-Noise-ratio of the receiver (SNR_{RX}).

$$S_r = k_B T_0 B_n SNR_{RX}$$

The required input SNR of a pulsed radar for a given probabilities of detection and false alarm depend on the target echo fluctuation characteristics, the number of output pulses processed before taking a decision and the processing gain for each pulse for matched-filter processing.

Thus, the range equation, written in terms of SNR as

$$R = \left[\frac{P_{TX}\, G_{TX}\, G_{RX}\, \lambda^2\, \sigma}{(4\pi)^3\, k_B\, T_0\, B_n\, SNR_{RX}\, L_{TX}\, L_{RX}} \right]^{1/4}$$

The equation resembles the link budget/SNR equation of a communication radio link with the notable difference that the dependence of the distance is on the inverse of the fourth power rather than the second power [3]. This is because unlike communications link, where the free space path loss is accounted for one-way, in a radar the loss occurs twice. B_n represents the amount of noise allowed into the receiver. It is different from the radar bandwidth B_r discussed in Section 2.2.1. Since PMCW radars have a wide baseband bandwidth, the noise allowed is also higher than FMCW and thus PMCW radars depend on the post processing gain to increase the SNR.

To further increase SNR of the system, MIMO techniques can be used as in communications transceivers [4].

2.6.2 Range Resolution

One of the important specifications for radar is the measurement of smallest distance of separation of its targets. This ability of the radar governs the Radar Bandwidth required for the system. By increasing the radar bandwidth (and thereby shortening the pulse width in time), we can effectively discern the two objects separated by a small distance R_{res}. The use of wider bandwidth increases the cost. Wider bandwidth radars are robust to interference from other receivers but can lead to an excessive range resolution which may have a detrimental effect on the sensitivity of the receiver [23].

$$R_{res} = \frac{C_0}{2\,B_r}$$

where, B_r denotes the Radar Bandwidth

For DMR, since the phase of the carrier is modulated like a digital modulation scheme, the sequence chip rate f_C determines the bandwidth of the modulated signal. If such a modulated signal is used for radar, then the modulating chip rate determines the signal bandwidth and hence the smallest range of measurement. With PMCW, every correlator runs on a one chip delayed version of the transmitted sequence ie delayed in time by the chip's period (Tc = $1/f_C$). Thus, for DMR, the expression for Range resolution and the radar bandwidth becomes

$$R_{res} = \frac{C_0}{2\,T_c} \; as \; B_r \approx f_C \; for \; Pseudo \; Random \; sequences$$

Unlike FMCW, the entire range of a DMR is quantized into Range gates. Due to the quantization of range, it must follow that the reflected waveform's power can vary due to the target's placement within a range gate. The range gates may not also be integer multiple of the wavelength of the carrier. Both these conditions enforce the requirement of a complex receiver architecture to recover the signal.

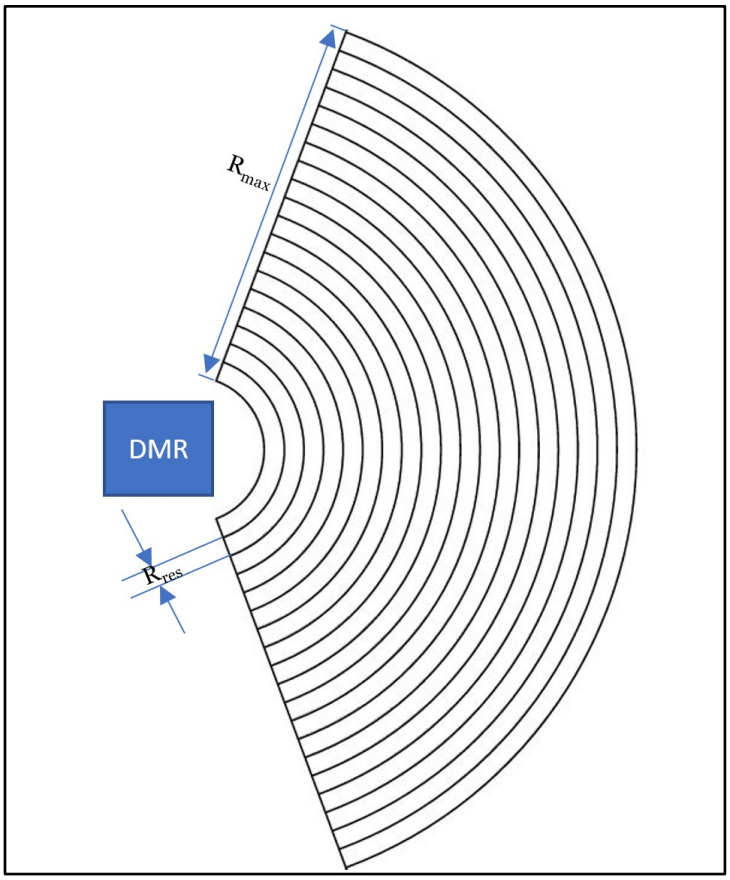

Figure 6: Range Resolution And Maximum Range Quantized in DMR

2.6.3 Angular Resolution

The ability to distinguish two objects of the same distance from the radar but separated by a small angle between them allows to identify radar targets spread radially. This parameter is determined by the antenna's half beam width also known as -3 dB bandwidth. Smaller beamwidth antennas have more directivity and hence more angular resolution [33]. The concept of angular resolution should not be confused with angular measurement accuracy, which for a single target is a function of antenna beamwidth and signal-to-noise ratio[8].

2.6.4 Maximum Unambiguous Range

The maximum unambiguous range of a radar is given by its ability to receive the reflected pulse completely before the next transmitting pulse. As shown below, the maximum range that the radar can unambiguously detect is linked with the Pulse repetition frequency. In DMR, however, the pulse repetition frequency is the sequence of length L_C repeating itself with a chip rate f_C. For clarity, a pulsed radar maximum range is shown [36]

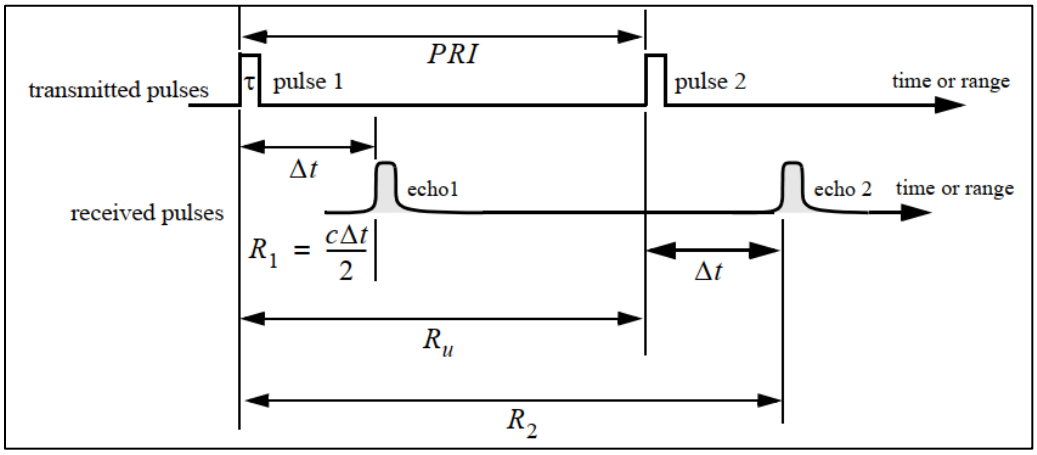

Figure 7: Pulsed Radar To Show the Maximum Range and Pulse Repetition Frequency [36]

$$R_{max} = \frac{C_0 L_C}{f_C}$$

2.6.5 Radar Cross Section (RCS)

The Radar cross section is the measure of the how big a target appears to the radar. The RCS of a target is the ratio of the incident power to the power scattered back from the receiver [55].

$$\sigma = 4\pi \frac{P_{s\_RX}}{P_{s\_TX}} \ (m^2)$$

where,

$P_{s_{RX}}$ – Power unit per solid angle scattered in the radar receiver direction,

$P_{s_{TX}}$ – Power per unit area in a plane wave incident on a target from radar transmitter

A target's physical size doesn't necessarily correspond to its RCS. RCS depends on many factors of the target: the material, the absolute size, the relative size of the object to the radar signal's wavelength, the incident angle and the reflected angle. RCS of human is approximately 0.16 m^2 (-8 dBsm) while a car can be varying between 10-100m^2 based on the angle of interception. The vehicle body, reflectors, radiator grill and license plate give a larger RCS for automobiles in general.

2.6.6 Target Velocity Resolution and Estimation

Radars measure the velocity of the target and distinguish stationary and moving targets by measuring doppler shift in the frequency of the carrier signal. By analyzing the detected signal's frequency change over multiple accumulations, it is possible to identify the target's velocity and direction. Doppler frequency separates the fixed targets from the moving targets and helps in assessment of the surroundings.

The operating principle is based on the doppler frequency shift of the carrier wave due to target's velocity. If a transmitter radiates a wave towards a closing in target, the received wavelength will be shorter and hence the detected signal will show the presence of the frequency shift.

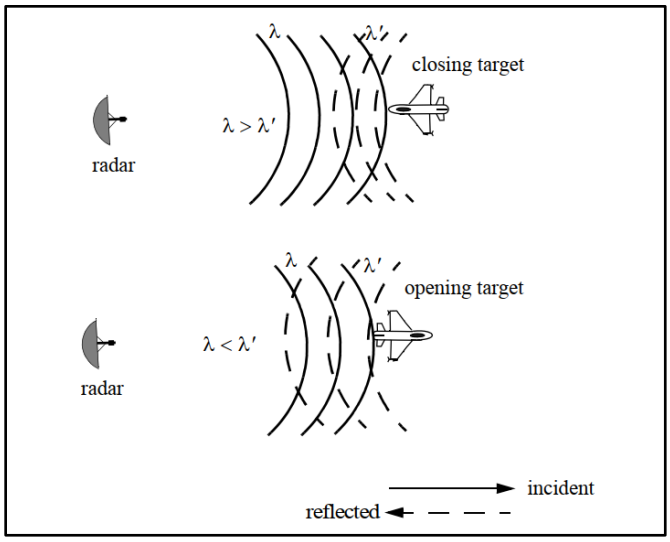

Figure 8: Doppler Effect Due to Closing In And Moving Away Targets [36]

The total phase change after the two-way propagation is

$$\varphi = \frac{2\pi}{\lambda_{\mathrm{RF}}}\, 2R = \frac{4\pi R}{\lambda_{RF}}$$

By differentiating this phase with respect to time, we get the angular frequency and the doppler frequency due to target's motion as below:

$$\omega_d = \frac{d\varphi}{dt} = \frac{4\pi v_r}{\lambda_{RF}}$$

$$f_d = \frac{2v_r}{\lambda_{RF}} cos\theta$$

In DMR, to visualize the target's movement, the resultant data after correlating for every range gate is stored and an FFT across N such samples show the frequency of the correlation peak and thus the velocity of the target.

As the correlation is performed over Lc range gates, the resulting FFT spectrum is a 2D matrix for length L_C and width N. Plotting of the the processed signal power vs each of the 2D axis gives the range profile and the velocity profile of the target.

2.6.7 Constant False Alarm Rate

Constant False Alarm Rate (CFAR) is the estimation algorithm used to detect and separate radar targets from the noise picked up from the environment. CFAR is used to set the threshold of the filtered signal in such a way that the radar receiver maintains a constant pre-determined probability of false alarm. There are different techniques to implement CFAR - adaptive threshold CFAR, nonparametric CFAR, and nonlinear receiver techniques [36]. Among them, Cell-Averaging (CA) CFAR technique is used in this model which is common for coherent radar.

Cell Averaging method uses adjacent cell's power level to create an adaptive threshold value to an optimal level. CA CFAR is based on two important assumptions. Firstly, each cell under test (CUT) of the 2D matrix of FFT data contains all the target's power for all the range gates. The choice of the number of guard cells and the reference cells on either side determine the fault probability P_{FA}. Secondly, the neighboring cells have the same statistical noise power level added due to clutter which is a zero-mean independent gaussian noise.

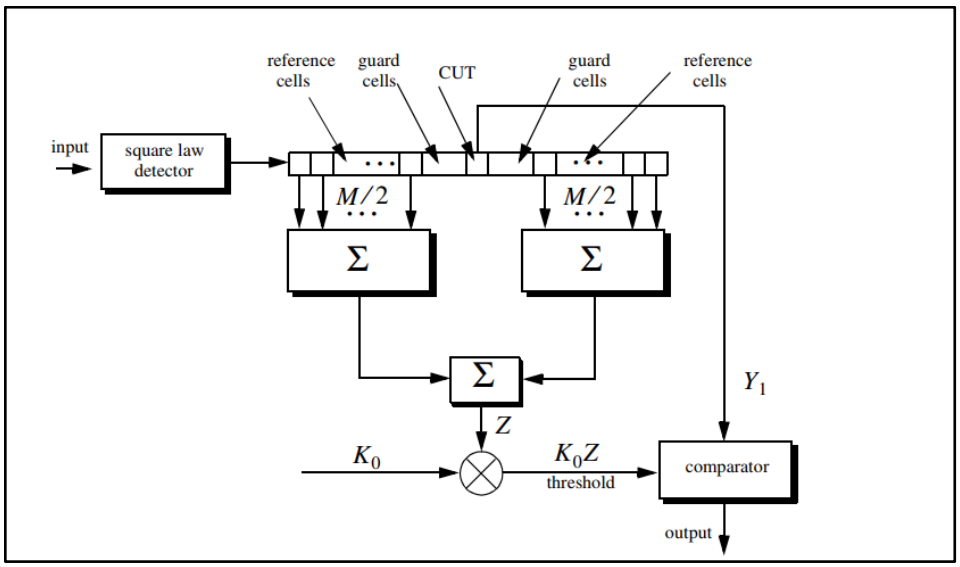

Figure 9: CA CFAR Detection Algorithm [9]

As shown in above diagram, the threshold (K_oZ) for each cell is dependent on the adjacent M/2 cells' average power. The average power of the reference cells

$$Z = \frac{1}{M}\sum_{i=1}^{M} x_i$$

With a gaussian noise variance in the cells as Ψ^2, the output power of the reference cells, Z, represents a random variable with a probability density function (pdf) with 2M degress of freedom. The pdf is

$$f(Z) = \frac{Z^{\frac{M}{2}-1} e^{-\frac{Z}{2\Psi^2}}}{2^{\frac{M}{2}}\,\Psi^M\,\Gamma\frac{M}{2}}\ ;\ Z > 0$$

With CA-CFAR, the probability of False alarm can be derived from conditional false alarm probability, which is averaged over all possible values of the threshold in order to achieve and unconditional false alarm probability. The conditional probability, however, can be written based on the algorithm, when y = V_T as,

$$P_{FA}(V_T = y) = e^{-y/2\Psi^2}$$

$$P_{FA} = \int_0^\infty P_{FA}(V_T = y) f(y) dy$$

where *f(y)* is same as the pdf *f(z)* without the scaling K_0

$$f(y) = \frac{y^{M-1}\, e^{-\frac{y}{2K_0\Psi^2}}}{(2K_0\Psi^2)^M\,\Gamma(M)}\ ; y \geq 0$$

Substituting, the value of *f(y),* the probabiliy of fault detection is,

$$P_{FA} = \frac{1}{(1+K_0)^M}$$

In radars, we usually start with a Probability of False Alarm (P_{FA}) spec, and to reach it, the scaling factor K0 is now found as

$$K_0 = P_{FA}^{-1/M} - 1$$

This approach creates a scaling factor for every cell that is independent of the noise power, which is the objective of CFAR processing [9].

2.6.8 Multiple Input Multiple Output (MIMO)

Collocated Multiple input multiple output systems increase the SNR of the system by the number of transmitters and receivers that work together as one big system creating virtual arrays. As explained in [58], we can create an $N_{TX}N_{RX}$-element virtual array by using only $N_{TX} + N_{RX}$ physical antenna elements.

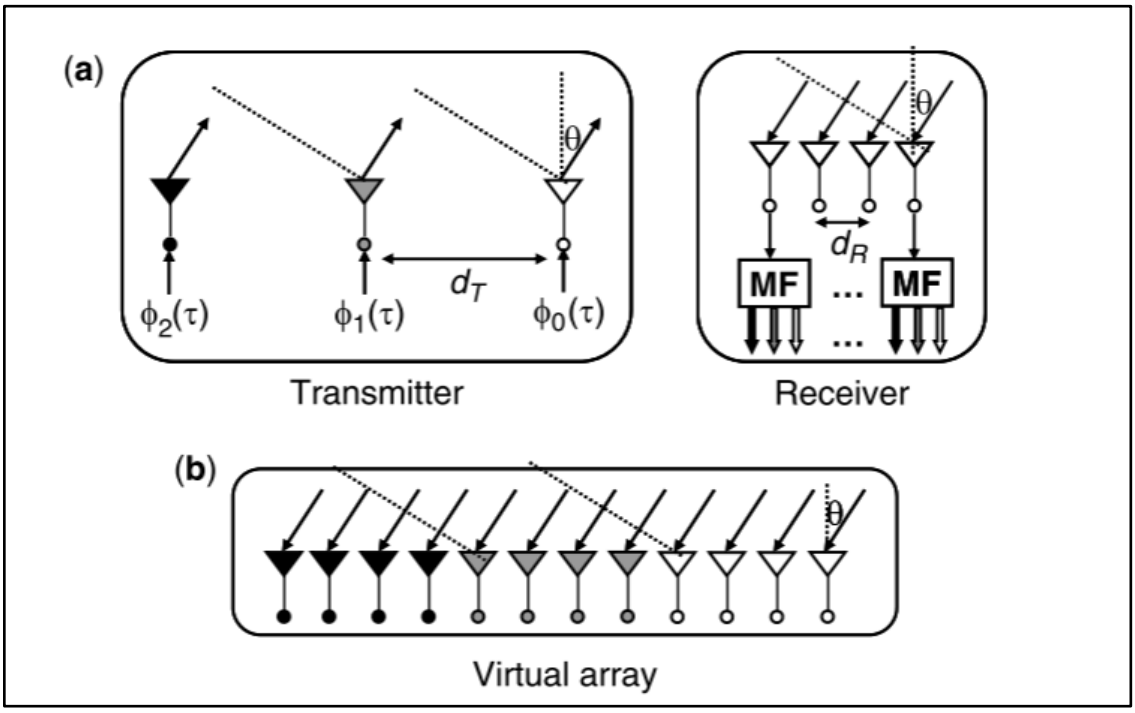

Figure 10: MIMO Virtual Array [58]

(a) Illustration of a MIMO radar system with $N_{TX} = 3$ and $N_{RX} = 4$;

(b) corresponding virtual array.

Due to Virtual Array of antennas, SNR increases as :

$$SNR_{MIMO} = SNR_{SISO} N_{TX} N_{RX}$$

$$N_V = N_{TX} N_{RX}$$

The ability of automotive radar systems to work in cascade is further enhanced as the codes of DMR can be aligned across multiple antennas and receivers of multiple radars.

Vito et al [16], describe the two different approaches for MIMO PMCW radars where as Oscar [18] proposes a third hybrid approach as well. In summary three different methods of MIMO is possible for DMR. They are :

- Sequence Engineering MIMO,
- Outer Code MIMO and
- Range Domain MIMO

Sequence engineering MIMO requires orthogonal sequences among different transmitters, it is possible to transmit and receive selectively from each antenna at each receiving antenna. But this approach creates a large sidelobe to the cross-correlation receiver and thus results in poor performance.

Outer code MIMO transmits the same sequence on all the transmitters after applying a zero cross-correlation transform to the sequences. A very popular transform is the Walsh-Hadamard transform. By transforming the sequence to every transmitter, each receiving antenna correlates the transmit sequence with N_{TX} sequence length. This produces NTX number of correlation peaks. Thus, this method effectively increases the SNR of the system.

For instance, if $N_{TX} = 4$, a 4x4 Hadamard matrix is applied to the sequence **S** of length L_C. Pictorially, this is clearly represented in [18].

$$H = \begin{bmatrix} 1 & 1 & 1 & 1 \\ 1 & -1 & 1 & -1 \\ 1 & 1 & -1 & -1 \\ 1 & -1 & -1 & 1 \end{bmatrix}$$

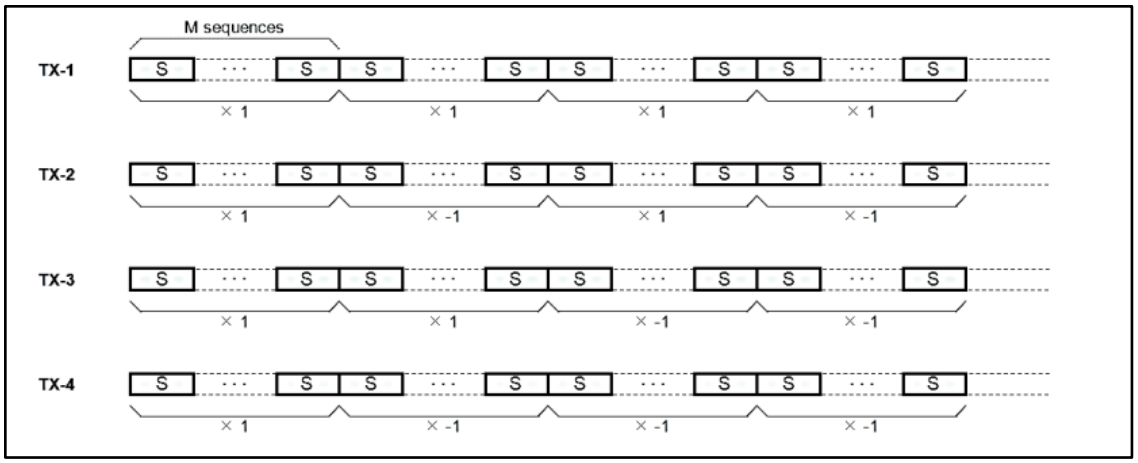

Figure 11: Hadamard Transform for Outer Code MIMO [18]

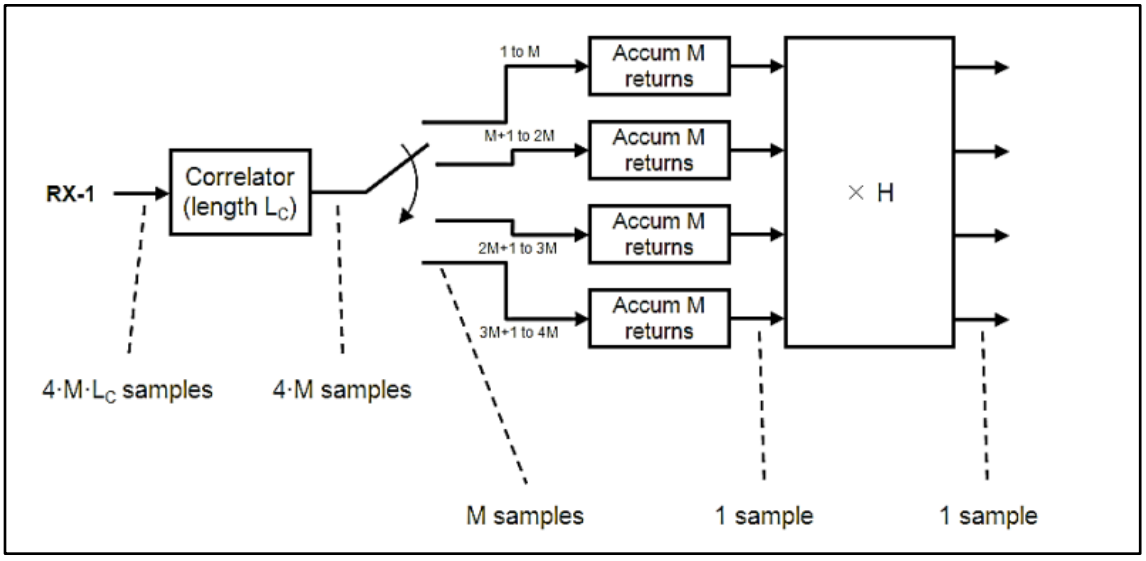

Figure 12: Outer Code MIMO Processing per Receiving Antenna [18]

Both approaches above produce strong correlation sidelobes that affect the radar performance. A hybrid approach is used with modification to the sequence length and using a zero-correlation transform, creating a Range Domain MIMO as in [18]. This method uses the same code on all the transmitters of initial length Lc required for the

range and range resolution specification extended by the number of the transmitter array.

$$S_{RD} = L_c \, N_{TX}$$

The orthogonality is introduced by using a Hadamard-Walsh transform of the extended sequence and by delaying the sequence that each transmitter transmits. The delay introduced in each transmitter is

$$S_{RDdelay} = \frac{Lc}{N_{TX}}$$

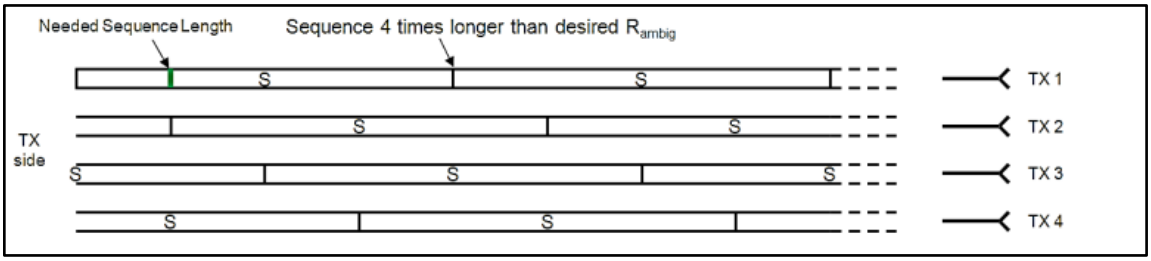

Figure 13: Range Domain MIMO [18]

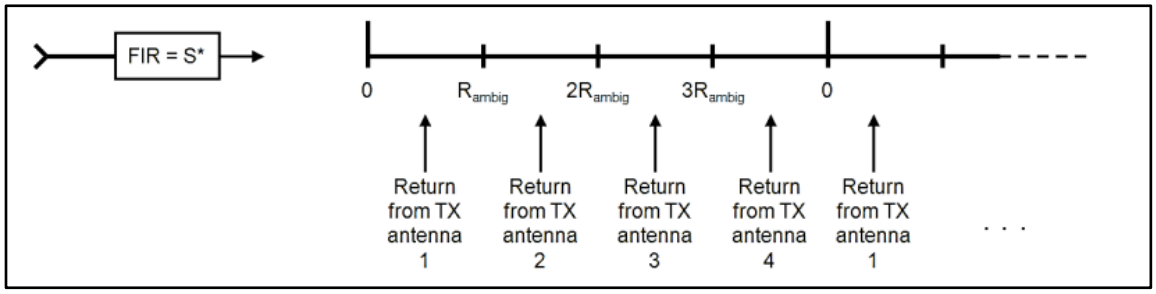

Figure 14: Range Domain MIMO Processing per Receiving Antenna [18]

2.6.9 Direction of Arrival

To detect an object in a 3D space, it is required to detect the range, the angle of elevation and the angle of azimuth. In an automotive application, it is required to detect the angle of azimuth as the elevation is usually not required. Direction of Arrival

detection is only possible with a MIMO system as the relative phase delay between adjacent virtual antennas now present a method to detect the signal.

So, for a typical MIMO radar data processing, the data consists of Range matrix (correlator output) for every range gate (1 to L_C), Doppler matrix (FFT output N) and the phase of the doppler matrix (angle of the target) per virtual antenna. Since each of this value exists for every range gate for DMR, the resulting matrices are arranged to form the radar data cube.

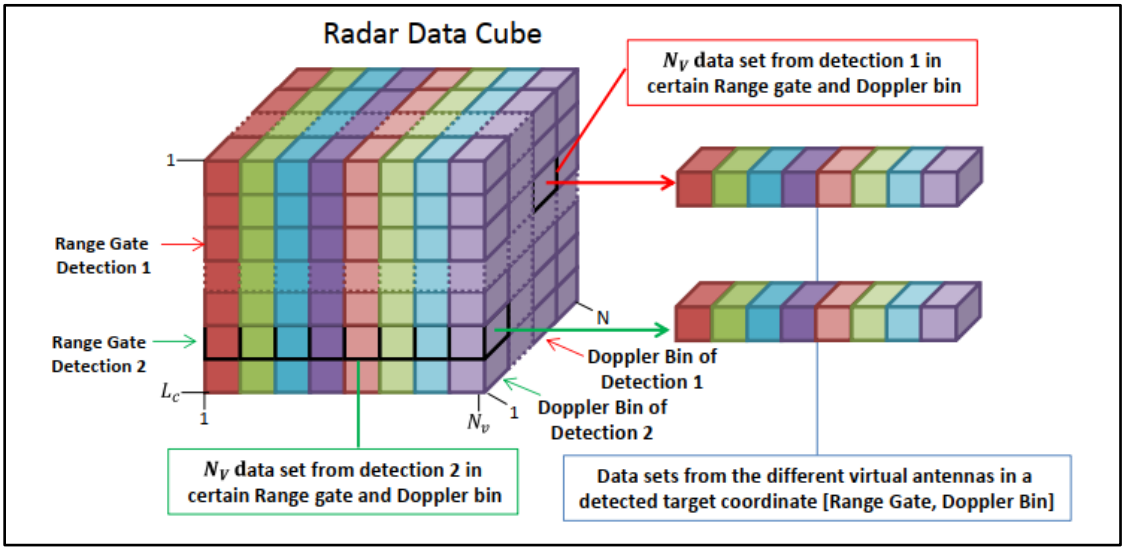

Figure 15: MIMO Radar Data Cube [18]

Beamforming of antennas can be done electronically using Phased Array antennas. In DMR, this is achieved by digital beamforming instead of the complicated analog/RF circuitry in FMCW radars. This digital beamforming in DMR is implemented in the system in transmitter and reverse in the receiver [18]. The delayed signal sequences in the MIMO transmitters can be visualized as the beamforming from the transmitter side. In the receiver, however, the signals coming in from the wanted direction are allowed and the other signals are attenuated. Implementation of this system is discussed in Section 3.7.6.

CHAPTER 3

SYSTEM MODEL OF DMR USING SIMULINK & MATLAB

In this chapter, the specific implementation of PMCW radar techniques using Matlab/Simulink for DMR is detailed. The architecture presented in [16],[17] detail the different modules in the transceiver for DMR. The approach in this work is to create a generic model that can be used for all three different radar types. So, the model is built for the widest bandwidth possible. The transmit and the receive RF sections may vary for the LRR due to higher power level requirements, but the baseband section is the same for all variants. The transceiver's architecture is similar to a digital communication system. The main difference, however, is the common LO used in the TX and RX mixer. By this alignment, there is coherent down conversion in the receiver and thus LO phase noise can be ignored [17].

Since the chosen modulation method is BPSK due to its higher noise tolerance than QPSK, there are many attempts to use higher modulation schemes [57]. There are attempts to use BFSK modulation schemes for Radar as well.

The model for DMR is represented in three forms:

a. Simulink based Complex passband model
b. Simulink based Equivalent baseband model
c. Matlab model

3.1 System Parameters

As radars can be used for different end uses LRR, MRR, SRR (Table 1) their parameters are changed according. Each type of DMR has a specific bandwidth and sequence length based on the requirement. The challenging case is the use of widest bandwidth for the

lowest return power level. SRR requires the maximum bandwidth and deals with very low RCS and therefore, very low power levels.

Parameter	Symbol	Value
Carrier Frequency	f_{RF}	79 GHz
Maximum Bandwidth	B_r	4 GHz
Chip Rate	f_C	2 GHz
Range resolution	R_{res}	75 mm
Max Range	R_{max}	37.5 m
Velocity resolution	V_{res}	0.25 m/s
Max Velocity	V_{max}	12.86 m/s

Table 2: System Specifications for a Typical DMR based SRR

To achieve the above specifications using DMR, a few parameters of the DMR should be calculated. Since DMR is built to be configurable, the choice of the parameters is important as many are interdependent.

For a single antenna TX-RX pair, the received power can be expressed using the Radar equation as:

$$P_{RX} = \frac{P_{TX} G_{TX} G_{RX} \lambda^2 \sigma}{(4\pi)^3 R^4 L_{TX} L_{RX}}$$

Taking the thermal noise addition due to antenna and the system into account, the signal-to-noise ratio for a SISO system is represented as:

$$SNR_{SISO} = \frac{P_{TX} G_{TX} G_{RX} \lambda^2 \sigma}{(4\pi)^3 R^4 L_{TX} L_{RX} (k_B T_0 B_n NF_{RX})}$$

where, P_{TX} is the transmitter power

G_{TX}, G_{RX} is the isotropic gain of TX, RX antennas,

σ is the RCS of the target,

L_{TX}, L_{RX} is the insertion loss of antenna in TX, RX sections,

R is the range of the target,

$k_B T_0 B_n$ is the thermal noise allowed into the system,

NF_{RX} is the input referred Noise figure of the receiver

To estimate the SNR for a particular scenario, let us key in system power and calculate the equation above. P_{TX} of a single transmitter is limited to 10 dBm peak power (for SRR) [16], with a RX System input referred noise figure of 10 dB for a RCS of -8 dBsm is below:

Transmit power	Ptx	10 dBm
TX antenna gain	Gtx,	3 dBi
RX antenna gain	Grx	3 dBi
Target RCS	σ	-8 dBsm
Path loss	$\frac{\lambda^2}{(4\pi)^3 R^4}$	-141 dB
Insertion Losses	Ltx,Lrx	-6 dB
Receiver power	Prx	-139 dBm
Receiver thermal noise with a Bn of 2.22 GHz	$k_B T_0 B_n$	-80 dBm
Receiver Noise figure	NF_{RX}	10 dB
SNR at RX input		-58 dB
SNR at ADC input	SNR_{SISO}	-68 dB
Required post process gain for SNR_{min}	G_{PostPr}	78 dB

Table 3: System Link budget calculation showing required post processing gain

[17]

The power gain in the RX chain is set at 30 dB as there is a strong reflection of the transmitted signal to the from the bumper of the car. To add to the complexity, the TX antenna's spillover to RX antenna can be as high as -30 dBm (considering 40 dB isolation between TX-RX antennas) and having higher gain in RX amplification can saturate ADC outputs.

The noise power at the input of the ADC is therefore,

$$N\_ADC\_in = k_B T_0 B_n + NF_{RX} + G_{RX} = -80 + 10 + 30 = -40 \text{ dBm}$$

Considering the input signal power of ADC to be 0 dBm (Full scale of the ADC), the noise floor of the ADC output (considering only quantization noise) is therefore,

$$N\_ADC\_Q = 0 \text{ dBm} - (6.02N\_b + 1.76)$$

Theoretically, if the quantization noise of the ADC is below the thermal noise of the system, then due to the random nature of the noise, the signal will be recovered from the noise floor in postprocessing. As Thillo et al conclude in [7] theoretically, an ENOB of 4 is all that is required of ADC. The main idea of DMR ADC is to have the quantization noise generated to be lower than the random noise power. The random noise quantized by the ADC will average out to zero and the postprocessing operations will improve the signal power greatly over the noise.

DMR's target signal can be recovered only with the post processing. To achieve the required post process gain, DMR uses correlation, accumulation of correlated outputs and N point FFT. The post processing begins with the ADC data correlated with the delayed versions of the transmit sequence, accumulation of correlator outputs for different range gates and performing an N point FFT on the accumulated results. The gain due to backend digital signal processing is thus,

$$G_{PostPr} = 10LOG_{10}(L_c MN)$$

In addition to this, MIMO operation increases the SNR by

$$SNR_{MIMO} = 10log_{10}(SNR_{SISO}N_{TX}N_{RX})$$

Implementation of Transceiver architecture to understand parts of the transceiver is done in Simulink and emulating the postprocessing of the model is performed in Matlab.

3.2 DMR System Parameters

Now, as discussed in the previous section, the sequence length L_C is available only for certain finite length for any PN code sequence, a choice is usually made to suit a code family for the scenario requirement.

For the system specifications presented in Table 2, based on the range resolution and doppler resolution requirements, the other important values are calculated.

The main limiting factor of DMR is the SNR_RX which is the noise power allowed into the system. Considering only the thermal noise, the noise equivalent bandwidth

Dwell time (Td) is the measure of time taken to collect reflections off targets and perform all the involved backend processing for a scenario and provide an SNRsys of 9 dB and better.

$$T_d = T_c\, L_c\, M\, N$$

Tc – Time period per chip

Lc – Length of the sequence

M – Number of accumulations

N – Number of FFT points

Typically, dwell time is calculated based on the SNRsys required from the processing gain (LcMN). Weaker target reflections from far ranges need more accumulation and the dwell time cannot be so long that the driver does not have enough reaction time for

corrective action. The maximum dwell time is limited to 10 ms as it is a good time to estimate the targets and present it to the autonomous driving system/driver.

Another interdependency is between the range resolution and the chip rate. The finer the range resolution the faster is the chip rate as they are related as

$$f_C = \frac{2R_{res}}{C_0}$$

Since the maximum bandwidth available for SRR & MRR is 4 GHz (77-81 GHz), the maximum chip rate is limited to 2GHz. This translates roughly to a range resolution of 75 mm with 79 GHz carrier wave.

$$R_{res} = \frac{C_0}{2f_C} = 0.075\ m$$

Thus, the highest resolution possible is roughly 3 inches. DMR can resolve objects separated with a distance of 75 mm from each other if the postprocessing gain achieves a SNR of 10 dB or greater for the received echo. Notice, by Radar equation shown in Section 2.2.1, the received signal power is also a function of the target RCS.

The maximum range that can be measured is derived from the R_{res} which sets the f_C as

$$\mathrm{R_{max}} = \frac{\mathrm{C_0}}{2\ \mathrm{PRF}}$$

$$PRF = \frac{f_C}{L_C}$$

Pulse repetition frequency inverse of the time taken to transmit L_C pulses by the transmitter at chip rate f_C. The maximum range that can be sensed will be the number of range gates that can correlate the entire sequence, which is L_C.

The above formula only holds for M-sequences. For APAS however, the $L_{Cactual} = L_{Ccalc}/2$ as discussed in Section 3.2.2. This might present APAS sequences as inefficient sequence as half the power is wasted compared to m-sequence. A relatively new code

sequence discussed for PMCW radars is the Zero-Correlation-Zone(ZCZ) which is not included in this work. ZCZ sequences have even better correlation properties, but available only at very select lengths and usable range is very limited.

To continue the dwell time calculation, the next part is to identify the number of FFT points needed. For each range gate, every L_C width of samples is correlated with the transmit sequence. The resulting values of correlated output(1 value) is accumulated over M times is stored as the first sample. This operation is repeated for N times to fill a row vector of 1 … N. Theoretically, for a L_C length sequence, the maximum number of range gates is L_C.

The necessity of FFT operation is to identify the target's velocity changes. A stationary target would produce only a peak at a particular range gate. When the target is moving, however, the correlation peak moves among several range gates. By identifying this, we can estimate the velocity and direction of the target.

So, the velocity resolution of the target determines the FFT resolution required and therefore the number of FFT points N.

$$v_{res} = \frac{\lambda_{carrier}}{2\,T_d} = 0.19\ m/s$$

For a dwell time of 10 ms, the range resolution is 0.19 m/s. The maximum velocity that can be seen by DMR will then be the target moving from one range gate to the other within the dwell time.

$$v_{max} = \frac{Rres}{T_d} = 7.5\ m/s$$

The ideal number of FFT points to detect the doppler frequency between these two velocity limits are given by

$$N = 2^{ceil\left(\left[LOG_2\left(\frac{2\,v_{max}}{v_{res}}\right)\right]\right)}$$

Based on the calculated required FFT points N, the value of number of correlation accumulations M are calculated for assumed dwell time of 10 ms.

For SISO, the rate of correlator output falls by a factor of 1/Lc and the output of the accumulator falls by 1/LcM. Hence, for SISO, at the end of FFT operation we are left with a 2D radar data cube that represents the target amplitude and velocity of size Lc x N. By setting a threshold for detection across the array using CFAR's Cell Averaging method, presence of targets among the clutter is uncovered.

Finally, based on the available values of the Lc, M and N, the new values of Rres, Rmax, vres, vmax are recalculated and fed back to the signal processing back end.

3.3 DMR Waveform Design

The choice of codes for phase modulating the carrier determine the performance of the DMR. Ideally, the codes are expected to have the same statistical characteristics as noise, perfect autocorrelation characteristics and perfect cross-correlation characteristics and available for all possible L_C values.

Perfect autocorrelation of sequences is required to match the transmitted sequence and the received signal thereby producing a peak indicating the delay. The rest of the range gates produce a cross correlation value below the Welch bound for the sequence. This ensures that the autocorrelation sidelobes do not disturb the peak correlation value to make the target to appear in more than one place.

Perfect cross-correlation of the sequences are required to ensure that the sequences used by one DMR does not produce a peak in the other DMR operating on different code that may or may not be of the same length.

No binary sequence can achieve perfect autocorrelation and cross correlation values [8]. Of the available pseudo random code sequences, this DMR model uses M-

sequences and Almost Perfect Auto-correlation sequences (APAS). A sequence known Zero-Correlation-Zone sequence (ZCZ) is attractive for PMCW MIMO radars [40] but not discussed here. Since DMR sequences are periodically transmitted, correlation of the transmit and receive signals can be implemented using circular correlation.

3.3.1 M-sequence

M-sequence is a binary sequence often known as pseudo-random noise sequences (PN)[3] that is generated using a linear feedback shift register configuration. The length of the sequence $L_C = 2^n - 1$, where n is the number of stages. The different feedback configuration and length of the shift register results is a unique generator polynomial. A generator polynomial describes the feedback loop and characterizes the sequence. The sequences have a good autocorrelation property, but they produce significant sidelobes. For weak reflections, the sidelobes powers can corrupt the cross-correlation results.

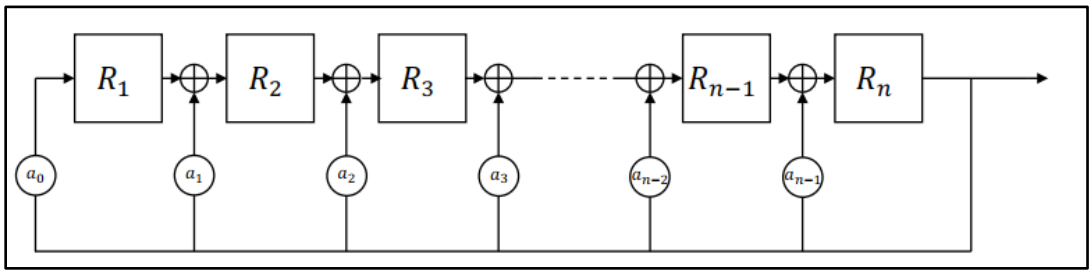

Figure 10: Galois Linear Feedback Shift register (LFSR) [40]

The periodic autocorrelation function (PACF) is a two valued function which returns the in-phase and the out-of-phase values for correlating a sequence to its delayed version. The in-phase PACF for M-sequence is Lc-1 while the out-of-phase value is -1. This cross-correlation characteristic makes M-sequence usable only for certain lengths. These are called as preferred m-sequences [40]. Non-preferred m-sequences have poor cross-correlation behavior.

In this work, preferred M-sequences of order(n) from 2 to 12 are used.

3.3.2 APAS

Almost perfect autocorrelation sequences were introduced in 1992 by Wolfmann[30] and recommended for PMCW radars by Thillo et al [31]. These sequences have good periodic autocorrelation property and have amplitude peak of L_C for a length of L_C. It produces zero out-of-phase for all lags except for +/- $L_C/2$, therefore making it useful for $L_C/2$ -1 range only. The sequence length has to be a multiple of 4 and $L_C/2$-1 must be a prime power.

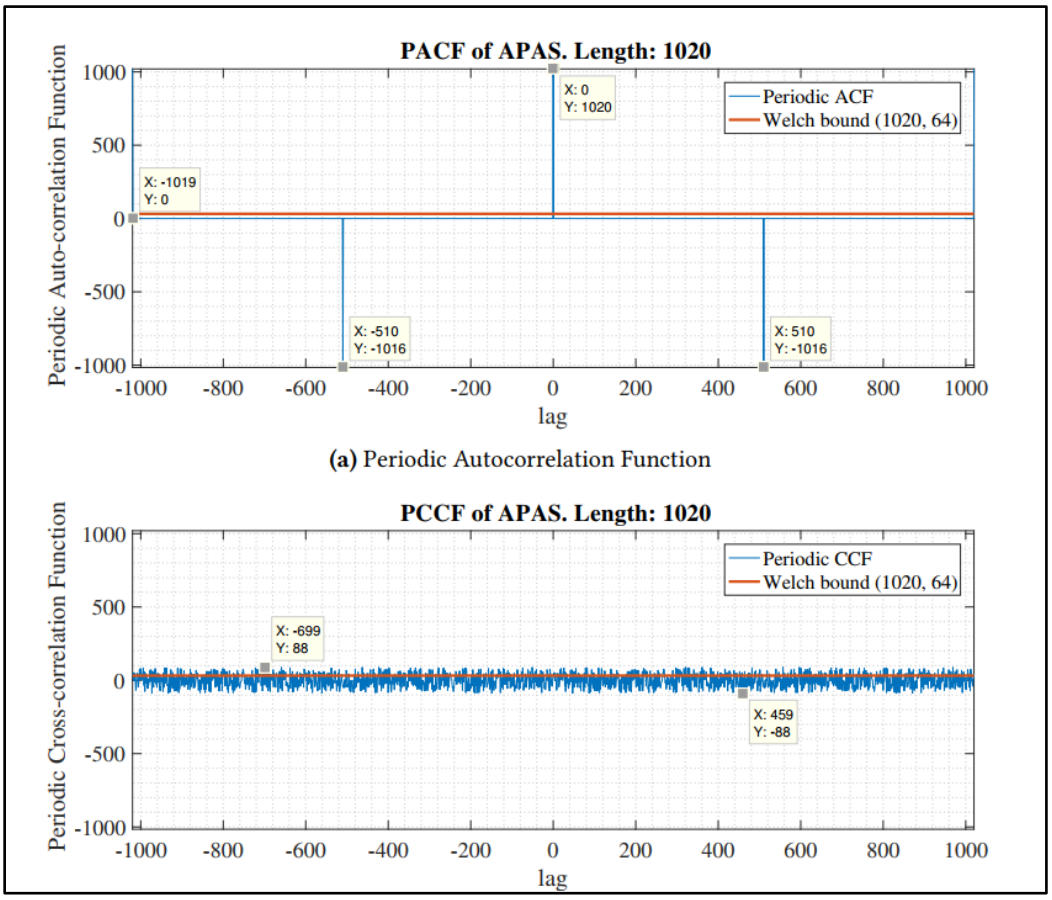

Figure 17: Periodic Correlation Functions of APAS [40]

3.3.3 Signal Shaping Network

A direct binary phase modulation using rectangular pulses at chip rate($1/f_C$) produces a main lobe bandwidth of $2*f_C$ as discussed in the Section 3.2. But this modulation also produces strong sidelobes [29]. The sidelobes' power level clearly violates the FCC/ETSI mask for automotive radars [25]. To stay within spectrum mask limits communication transmitters, use many techniques to suppress the harmonics of the baseband signals thereby reducing the sidelobes [27],[28]. One of the most widely used technique is to filter the BPSK signals to reduce the high order harmonics.

As used in [16], this model attempts to reject the 3rd order harmonics and attenuates higher order harmonics. This shaped baseband BPSK signal is used as the modulating signal for the DMR.

3.4 Transceiver Architecture in Simulink

As PMCW radars have a very wide signal bandwidth, Direct conversion architecture are favored. The direct conversion receivers eliminate the requirements of IF processing but introduce second-order problems. The main problems with Direct Conversion receivers are LO radiation and leakage from RF port to LO's VCO.

The chip rate f_C is usually a derived of the system's main clock. This clock is also multiplied to produce the system's carrier clock to reduce the LO radiation. Leakage from RF port to LO can be reduced using a multiplier VCO to produce LO. This Direct conversion transceiver model is implemented with programmable non-linearities at the LO. To solve above two problems of Direct conversion receiver, the system is assumed to use a Sub Harmonic Injection Locked Oscillator (SH-ILO) as in [16]. The impedances and Noise figure of the entire chain are estimated using hand calculations and verified with RF Budget Analyzer in Simulink.

The transceiver's model is built using Simulink platform as it provides an intuitive interface to build and simulate the model. Specific to radar, the platform also supports standard mathematical models for free space channel attenuation, stationary and moving radar targets, processing signals in the MATLAB and RF domain and ability to integrate custom MATLAB functions.

Simulink can perform transient simulations that provide a good understanding of the interconnection between modules and provides the ability to explore different architectures. The aim of the thesis is to understand the requirements of individual block specifications of DMR and the programmability of the Simulink model enables this.

The model represents an initial idea of the system with multiple targets, waveform design and spectrum of the transmitted waveform. The model includes a sequence selection script that invokes the Simulink model with appropriate sequence length for the target specifications. The sequence is repeated for the entire dwell time calculated for the specifications. The model thus includes a triggered sequence generator, waveform design to meet the spectrum mask, RF up conversion, Free space channel, target(s), RF signal and noise reception with non-idealities, RF quadrature down conversion and Digital conversion of the received signal. The In phase (I) and Quadrature(Q) down conversion are necessary as there exists a random phase reflected off the target based on its position and velocity. A complex baseband signal is evidently more useful in the detection of the target's distance and velocity even in FMCW radars [13][14].

The system is also required to be comply the FCC/ETSI regulations for the automotive radar to operate in the allocated 76-81 GHz. The baseband envelope of APAS and M-sequences are shown as below. Clearly, the sidelobe power levels exceed the

regulatory specifications. A method to reduce the sidelobes is presented in [16]. There are many methods in literature to reduce the sidelobes of BPSK signal.

To be able to sample the ADC at the same frequency as of the chip rate is optimal in DMR, as the interest is more on the levels of the received signal rather than the shape. In FMCW radars, the received waveform's shape determines the doppler and the range resolution. Hence, FMCW radars employ sigma delta ADCs to accurately reproduce the beat frequency waveforms in discrete domain.

Unlike high speed communication links, DMR uses BPSK signals that are the least affected due to random noise as their constellations are at the maximum farthest. During every stage of signal processing, the signal adds up coherently while the noise voltage adds in a random uncorrelated manner. This difference between signal and noise summing power over each post processing operation (correlation, integration and FFT) improves and the signal is recovered from the noise floor.

Guermandi et al[17] claim that though the RF mainlobe bandwidth of the system with a chip rate of 2 GHz due to the digital modulation, is 4 GHz. The authors claim that this spectrum can be digitized by an ADC sampling at 2 GHz as we are interested in the signal levels and not on its shape as in FMCW IF. This has been accomplished by aligning the sampling clock to the fall exactly at the middle of the received chip sequence. While this may appear to be a sub-sampling approach, the requirement for this receiver is to detect the levels only as the doppler and MIMO processing is performed after the correlation.

The idea of aligning the ADC sampling to the middle of the received sequence may produce the highest SNR only if the target is exactly in one of the range gates. Since the system also uses Complex sampling, the detection will still happen albeit at differing power levels based on the position. Since automotive radars are based on the assumption

that either the target or the radar is under constant motion, location of the targets will fall into the range gates thus ensuring a higher SNR in one of the many frames per dwell time.

To align the sampling edges in simulink, blocks triggered with clock edges have been used. It is assumed that the clock of the sequence generator is a divided down version of the system PLL clock. The LO is a multiplied version of the main clock and shared between transmitter and receiver. The target is also placed at random distances from the radar for the simulation of all scenarios and not necessarily an integer multiple of the range gate. A rising edge triggered sequence generator and falling edge triggered ADC sampling is used to align the sampling edge to the middle of the received sequence.

3.5 Model for ADC

The main objective of this work is to determine the sampling frequency and the ENOB of the ADC required to make the system work with non-idealities – finite IP3, jitter in clock, I/II order filter for down conversion filter, Nonlinear power amplification in the transmitter etc.

Though, Guermandi et al [17] use 7 bits in their work and though, theoretically, Thillo et al [27] conclude that 4-bit ADC should be enough, this work seeks to find that it is rather necessary to have higher number of bits. Since the number of ADC bits determine the bit width of all subsequent stages, care must be taken to not allocate more bits than necessary. The ADC and the correlators (matched filter for each range gate) along with the sequence generator run at f_C (the highest frequency in the baseband), so care must be taken in deciding this.

The ADC's ENOB should also enough accurate to represent the noise power in the system, which can be filtered with correlation and accumulation.

As the signal bandwidth can be as high as 4 GHz and a 2 Gsps ADC is required with low latency, there are many choices for high speed ADCs. Among Time Interleaved SAR ADC, Folding and Interpolating ADC and VCO based ADC, pipelined cyclic ADC is chosen for its low latency and accuracy and flexible sampling rate [32].

3.5.1 Architecture of Cyclic Pipelined ADC

A block diagram representation of cyclic ADC is shown as below

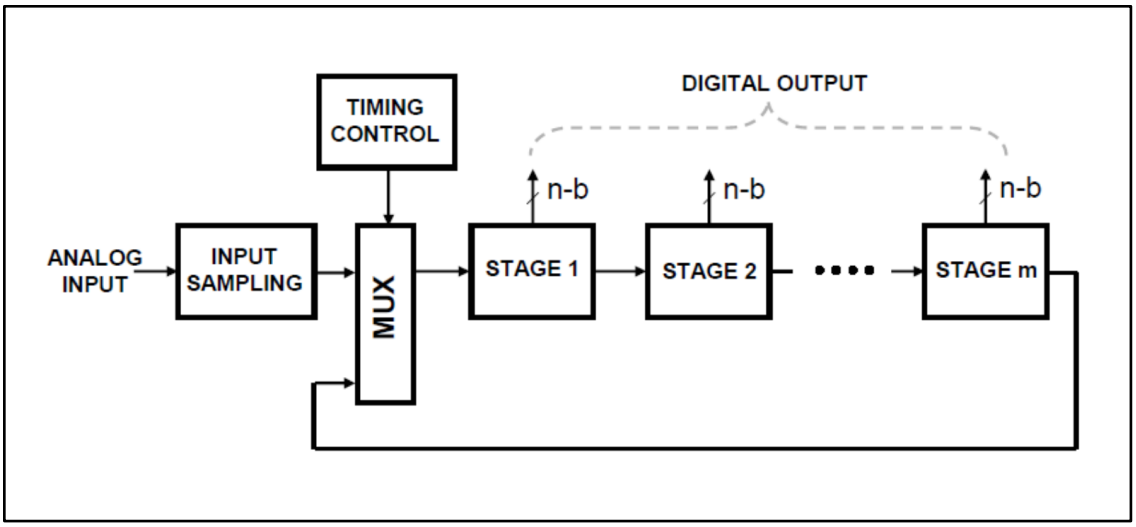

Figure 18: Cyclic Pipelined ADC block diagram [61]

The cyclic RSD ADC operates by sampling the input periodically at a clock timing controlled by a timing control. After sampling the input, the ADC converts the analog voltage into its digital equivalent over multiple stages and clocks. Each stage consists of a Redundant Signed Digit (RSD) ADC stage working on one of the two phases of the ADC clock. The digital equivalent of the analog residue signal from each stage is then delayed and aligned arithmetic sum of all the digital conversions. For an ADC of N bit accuracy, the cyclic ADC uses only N/2 stages, if the input sample is fed to the first stage on one phase of the clock and the residue of the last stage is fed on the other phase. Each RSD stage can be designed to process the signal within a half clock period by using switched capacitor networks for comparators and residue amplifiers [33].

Pipelined ADCs can be explained by considering a two-step Flash ADC to convert an input signal in place of one step Flash ADC using 2^N-1 comparators. By doing so, each Flash ADCs use nearly half comparators instead of using one flash ADC of 2^N comparators. The first ADC is usually known as the coarse ADC and the second as fine ADC.

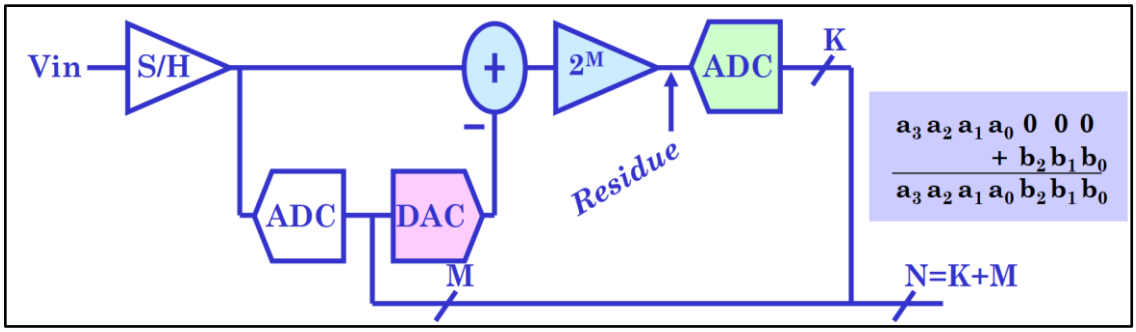

Figure 19: A Two-step Flash ADC architecture [61]

The problem, however, in such an arrangement, to use lesser comparators we ended up with the requirement of additional circuitry. The coarse ADC outputs are converted back to analog using a DAC. This DAC is expected to have a lower quantization error to reconvert the coarse ADC output and recommended to be at least twice linear than the coarse ADC bits M to represent the analog signal accurately. The resulting signal is amplified to bring out a residue voltage. This residue which is converted to by the fine ADC to K bits. The outputs of both ADCs are the weighted sum of both ADC outputs.

Pipelined ADCs are an extension of the of two-step flash ADC idea of using just single bit ADCs. They operate by comparing the input against reference voltage and a residue voltage is generated which is a sum of input voltage amplified twice and an additional +/-Vref based on the comparison. This residue voltage is fed to next stage and the cycle repeats for N stages. The Vref levels and the number of stages considering the

Full-scale reading FSR of the ADC and the number of stages. The last stage of pipelined ADC is usually a flash ADC to save one clock phase latency [33].

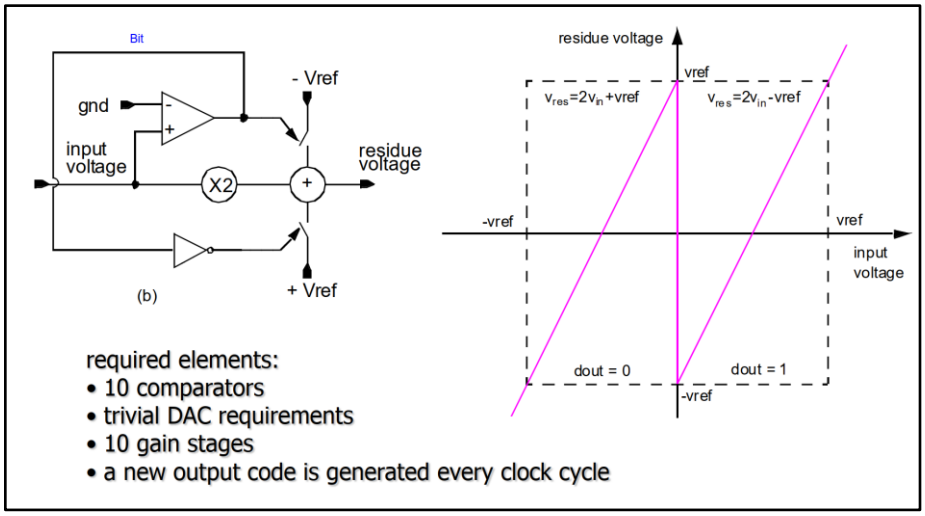

Figure 20: 1 Bit Stage for pipelined ADC [61]

This 1-bit pipelined stage suffers from comparator's non-idealities and the amplifier's finite bandwidth which affects the transient settling behavior. Comparator offset produces out-of-range residue voltages and can result in missing and/or redundant codes. Finite offset of the amplifier can result in missing codes due to loop offset. To mitigate this problem, a redundant signed digit is added by introducing two level comparison to generate the residues. The comparison limits are changed to include three levels, -Vref to vl quantized as bits 00, vl to vh to bits 01 and, vh to +Vref to bits 11. The input is multiplied twice and added Vref, 0, or -Vref accordingly.

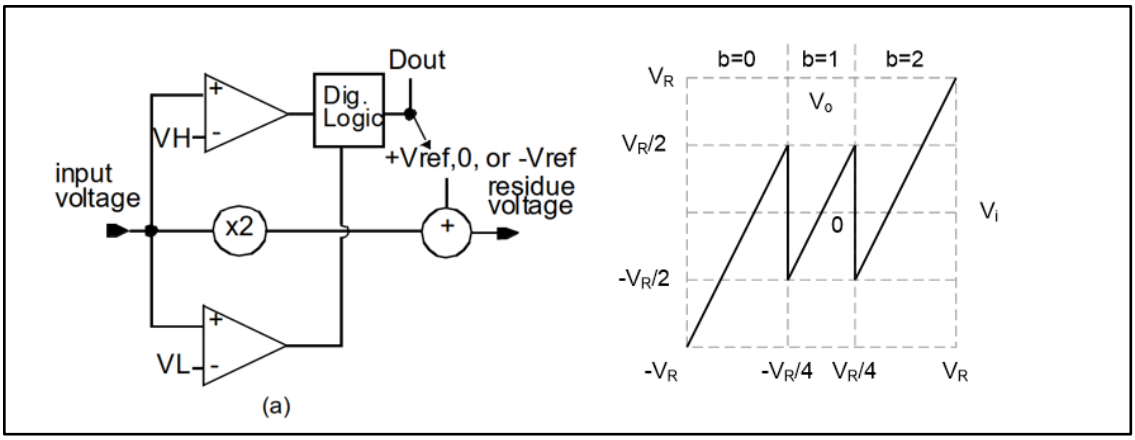

Figure 21: 1.5-bit RSD Stage for Pipelined ADC

Modifying the threshold levels gives the advantage to deal with amplifier's finite bandwidth, offset and comparator's offsets in avoiding creating out-of-range residue voltages for the subsequent stages. The ENOB due to three decision levels is now $ENOB_{1.5bit} = log_2 3 = 1.58$, hence known as 1.5bit RSD stage.

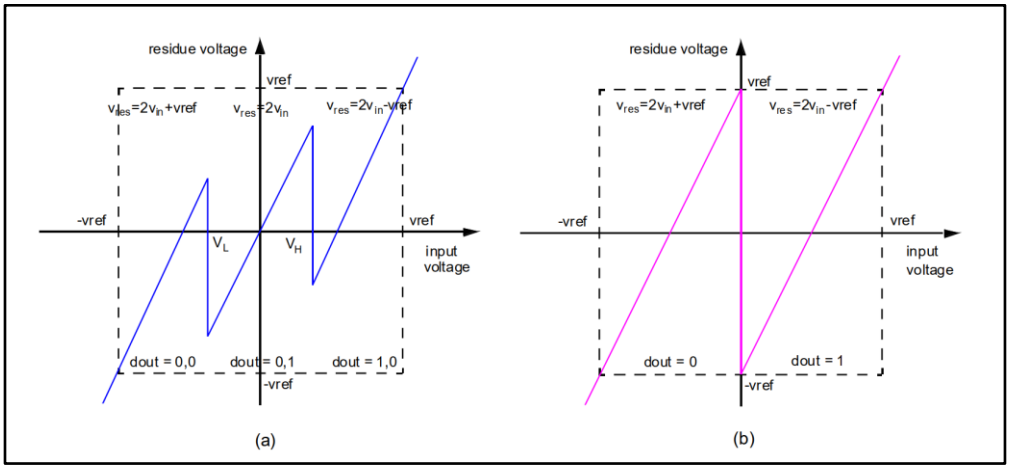

Figure 22: Advantages of Redundant Signed Bit stages [61]

A flowchart representation of a single 1.5bit RSD stage is shown as below.

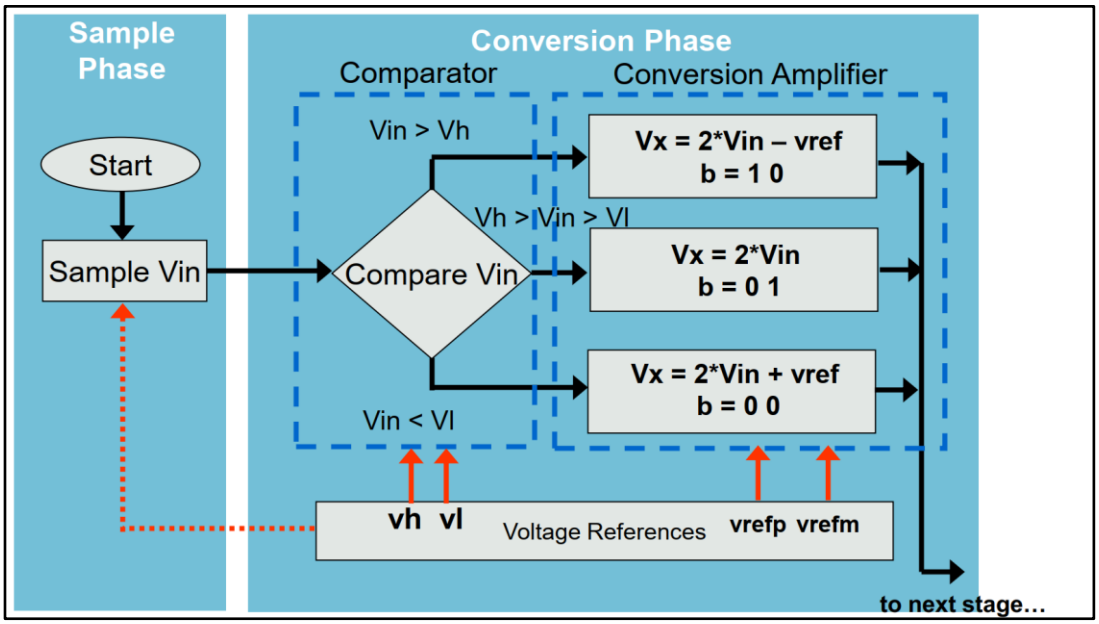

Figure 23: Flowchart of 1.5 Bit RSD Stage Operation [61]

The bit pairs of each RSD stage are added positionally with an overlap[33] to create the final word of the RSD stage. A simplified single-ended 1.5bit RSD stage is shown below using switched capacitor circuits, opamp, comparators and digital logic. Actual designs use a differential version

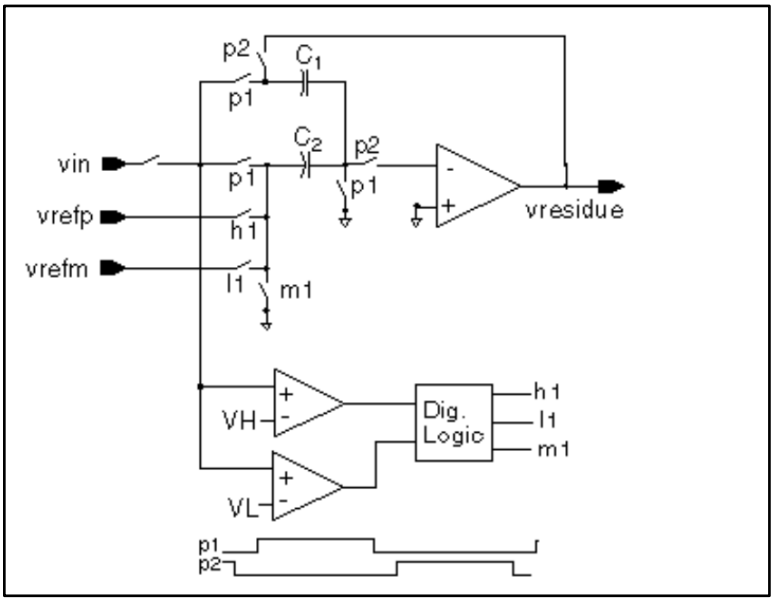

Figure 24: Simplified schematic of 1.5-bit RSD Stage

$$v_{residue}^{P2} = v_{in}^{P1} z^{-\frac{1}{2}} \left(1 + \frac{C_1}{C_2}\right) \mp \left([V_{refp}, V_{refm}], 0\right) \left(\frac{C_1}{C_2}\right)$$

The RSD stage's accuracy is still dependent on few more parameters due to this architecture. The matching between capacitors C1 and C2 and the Gain of the amplifier (A_v) determines the accuracy of the residue.

$$v_{residue}^{P2} = [v_{in}^{P1} z^{-\frac{1}{2}} G_{vin} \ \mp \ \left([V_{refp}, V_{refm}], 0\right) G_{vr}] \ [\frac{A_V \beta}{1 + A_V \beta}]$$

where

$$A_v(s) = \frac{A_{v0}\left[1 + \frac{s}{\omega_z}\right]}{\left[1 + \frac{s}{\omega_{p1}}\right]\left[1 + \frac{s}{\omega_{p2}}\right]}$$

$$\text{where, } G_{vin} = \left(1 + \frac{C_1}{C_2}\right)$$

$$G_{vr} = \frac{C_1}{C_2}$$

$$Feedback\ factor\ \beta = \frac{C_1}{C_1 + C_2 + C_{px}}$$

The mismatch between the capacitors due to layout extracted values can be used to calculate the performance of the ADC.

The use of MOS devices as switches adds thermal noise power that gets sampled onto the capacitors. This noise power affects the voltage accuracy and the resistance value affects the voltage settling accuracy of the RSD stage. The generic equations for minimum amplifier Gain and the unity gain bandwidth are:

$$A_v = \frac{2^N}{\alpha}\left(\frac{1}{\beta}\right)$$

$$UGBW \ \geq \ -\frac{log_e\left[\frac{\alpha}{2^N}\right]}{2\pi t}\left(\frac{1}{\beta}\right)$$

where, A_v - minimum required DC Gain of each stage,

N - Number of Bits yet to be resolved in the subsequent stages,

α - Required Stage accuracy in fractions of an LSB (eg: 1.0, 0.5, 0.25, 0.125),

β - the Feedback factor,

$UGBW$ - Unity Gain Bandwidth,

t - Time available for settling (Generally, half the clock period).

The equation for calculating switch resistance for each stage is given as

$$R_{on} = \frac{-t}{log_e(\alpha\ LSB)\ C}$$

where, R_{on} - On resistance of the Switch,

t - Time available for settling (Generally, half the clock period),

α - Required Stage accuracy in fractions of an LSB (eg: 1.0, 0.5, 0.25, 0.125),

LSB - Resolution of the ADC,

C - Capacitance in series with the switch.

As we proceed in the stages, the resolution of the ADC reduces and allows to use MOS switches with higher Ron without sacrificing accuracy.

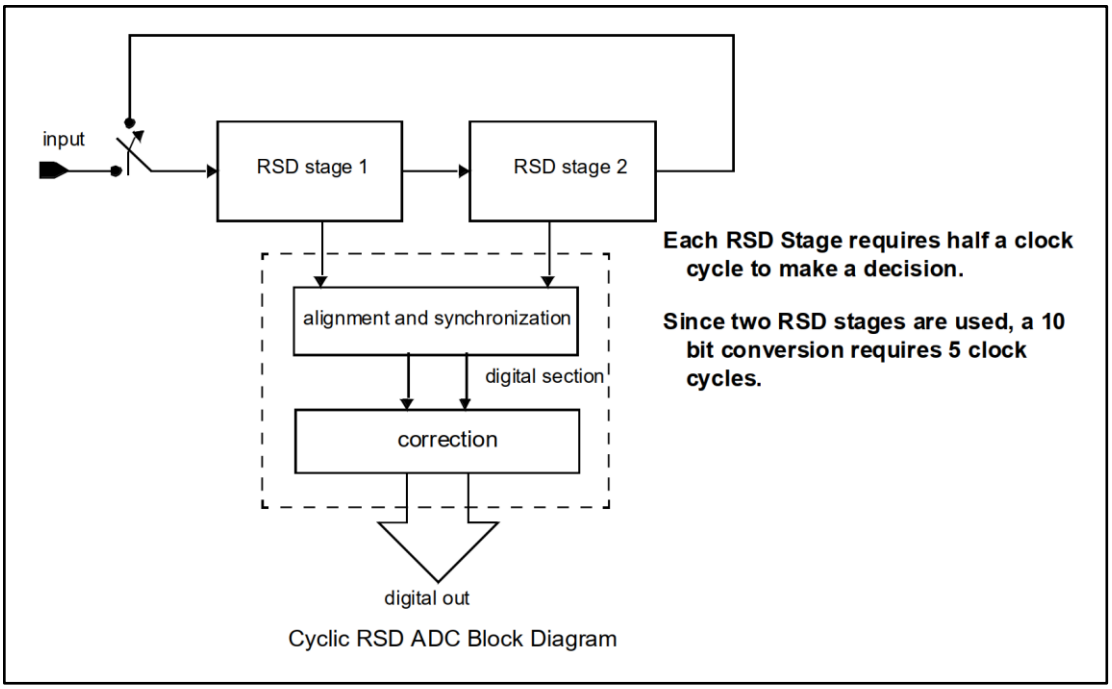

Figure 25: Cyclic Pipelined ADC [61]

The conversion happens as follows

1. At the first clock edge of the timing control, the input is sampled on to the Sample and Hold Amplifier (SHA) and fed to stage 1.
2. In the next clock phase within the same clock period, stage one receives the stage N/2's residue and propagates the residue to 1.5bit conversion stages for another N/2 stages taking N/4 clock period
3. This method produces the output for the input with a latency of N/2 cycles of T_C. (RSD stages are clocked at $T_C/2$ and it takes N/2 cycles to propagate N stages)
4. The digital alignment and error correction logic for all the N stages add up as below. Each addition is realized with a full adder.

B_{11}	B_{12}							
	B_{21}	B_{22}						
		B_{31}	B_{32}					
			B_{41}	B_{42}				
				…	…	…		
					…	…		
						…		
						…		
						$B_{(N-1)1}$	$B_{(N-1)2}$	
							B_{N1}	B_{N2}
Bit_N	Bit_{N-1}	Bit_{N-2}					Bit_1	Bit_0

5. An N stage pipelined ADC would require the same power and the time for a cycle to convert the input, but the cyclic ADC wins as it employs only N/2 stages and takes half the area needed on the chip.
6. Without much changes to the digital alignment and synchronization, cyclic RSD ADCs can be extended easily to in even number of ADC Nbits.

3.5.2 Matlab Model for Cyclic Pipelined ADC

A standalone model for this type of cyclic ADC has been developed by NXP and has several non-idealities included. Matlab models execute faster and can produce the same characteristics of the ADC modeled using Simulink [34],[35]. The non-idealities of the ADC are programmed into the model are capacitance mismatch, common model voltage offset and Finite op-amp open loop gain. The model is also modified such that it can work with an array input when used with the standalone matlab model.

This custom matlab model is integrated to the DMR's Simulink model as a triggered subsystem. The clock is derived from the RF section's LO clock signal. To complete the ADC's non-linearity, a random jitter model is implemented in Simulink based on [35] with finite rise and fall times of the clock signal.

3.6 Simulink Model for DMR transceiver

The transceiver model is built with modules described so far in this chapter. High frequency RF modules are modeled using RF blockset toolbox. The RF blockset models can simulate the high frequency components with non-idealities faster and in a memory efficient way. The toolbox also includes all the basic components needed for building the system. There are two effective ways of simulating the system with a RF blockset transceiver – passband model and equivalent baseband. Transferring from and two between Simulink environment signals to RF blockset uses simRF's inport and outport.

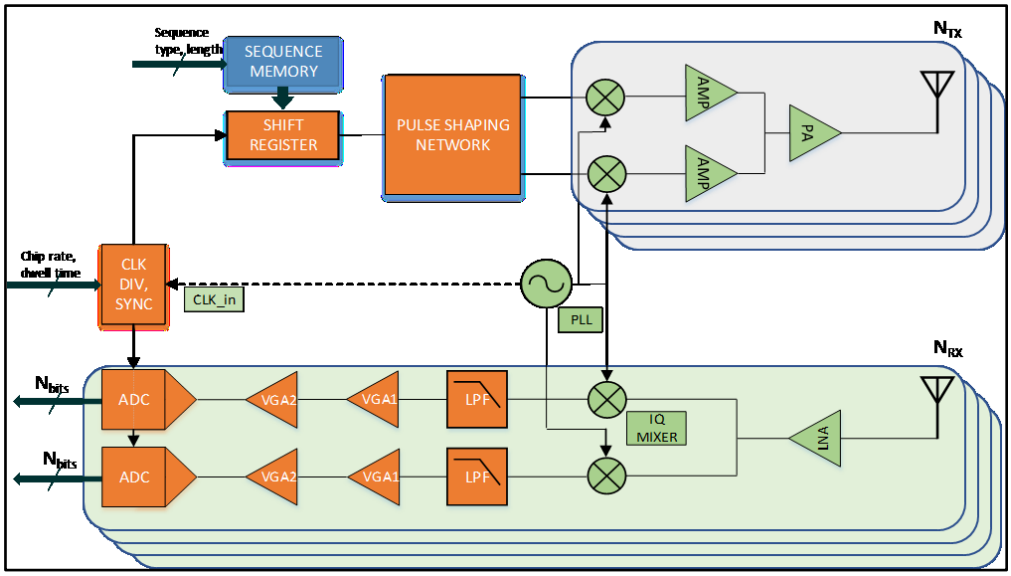

Figure 26: Block diagram of Proposed DMR model

3.6.1 Passband Model

The passband model simulation of the transceiver takes the model through all the possible time steps required for the system. As expected, this is the slowest form of the model to simulate. These models help understand the system thoroughly. Many points at the system can be probed. For instance, the spectrum of the transmission, the behavior

of the LNA with a noise figure and finite IP2/IP3 and the power gain of the entire cascade.

The filtered BPSK baseband signal is modulated on a real carrier and transmitted to the free space after power amplification. The simulation shows the lowered sidelobe power levels that fit the spectrum mask requirements. The radar target models and the free space channels are derived from the Phased Array Toolbox which is also an industry standard for radar simulations. The passband model is built as below:

Baseband modeling:

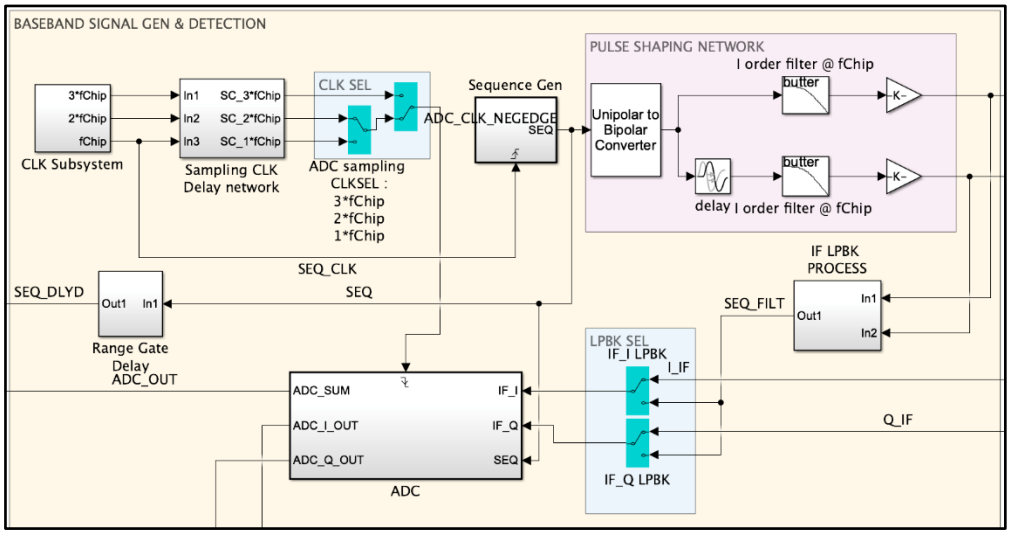

Figure 27: Baseband Section of DMR Simulink Model

The timing of the sequence generator and the ADC sampling is aligned to a global clock. The sampling frequency of the ADC is higher to accommodate the cyclic ADC. A Clock select switch arrangement is present in the model to modify the ADC sampling if other architectures are chosen. The sequence generator can use M-sequences or APAS based on a programmable variable before the start of the simulation. The length, and the characterizing polynomial of the sequence can be programmed as well. The model can be extended to include newer high correlation sequences that are in active research such as Zero Correlation Zone sequences etc., A simple I order pulse shaping network is

implemented as discussed in [16]. Loopback paths are present to characterize ADC based on sequence or external inputs.

The custom matlab ADC model is included with a programmable ENOB and non-idealities working on the falling edge sample of the input. The ADC sum represents the complex ADC data that is dumped to the simulation workspace for postprocessing.

RF Modelling:

The filtered baseband sequence is converted to RF domain using Simulink-RF sensors. The sensors convert the sequence as ideal voltage or power signals with impedances. The RF blockset includes the Thermal Noise, non-idealities of Amplifiers, Mixers and Summing junctions. Impedances of the transceiver chain is matched to 50 ohms.

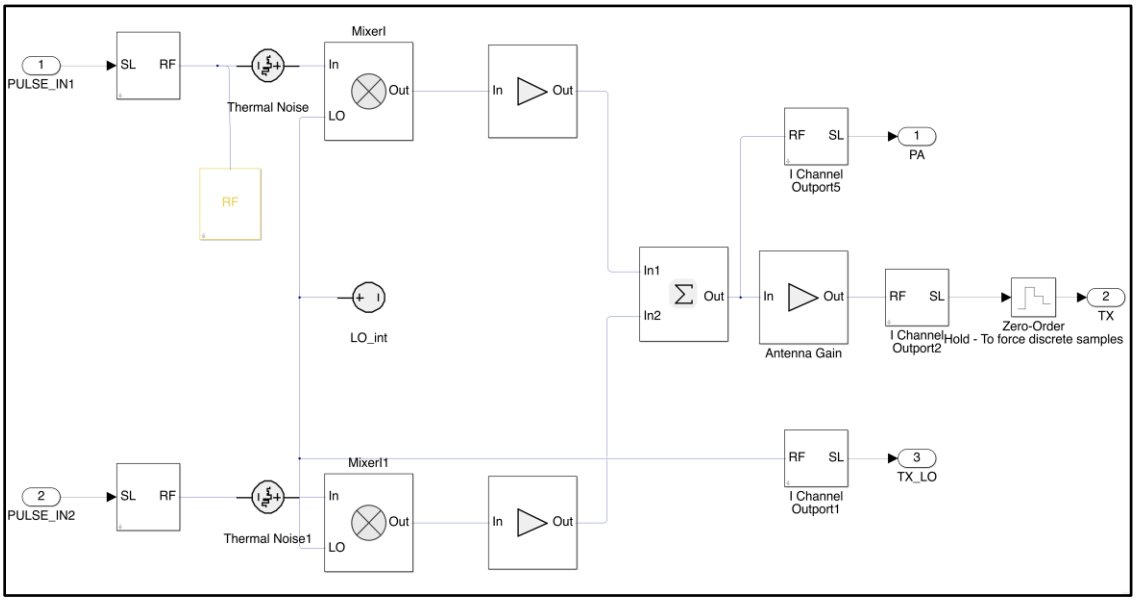

Figure 28: Simulink model of DMR TX using RF Blockset

Similar approach of modeling is followed for the receiver side of the model. Since DMR requires the down conversion with the same LO as the transmitter, an interface port is present on both blocks to share the LO signal.

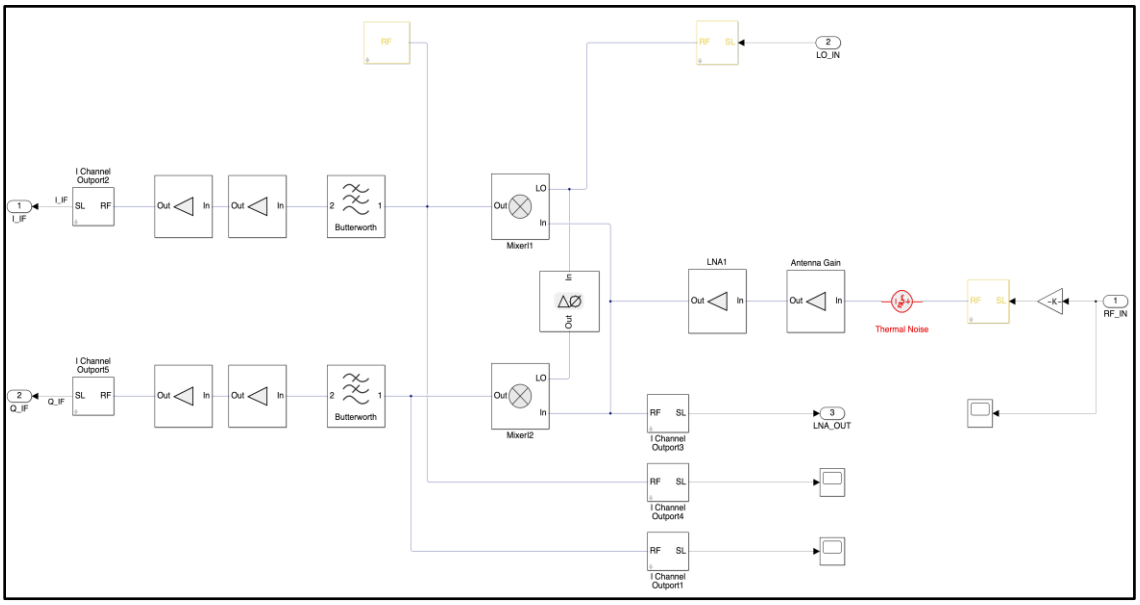

Figure 29: Simulink model of DMR RX using RF Blockset

The outputs of TX block are converted to Simulink datatype and measured for the signal spectrum and bandwidth requirements set for Automotive Radars by the American and European standards committee. The separate models are all now hooked up together to realize the complete system.

The complete model is shown in Figure: . The model uses the Simulink's Phased Array toolbox to model the Free space channel. As the reader would notice, there is only one instance of Free space channel and no Free space after the target. Mathworks recommends using one instance of Free space channel with two way propagation model for accurate modelling of time delay and attenuation incurred on the transmit signal. Multiple scopes and Spectrum Analyzers can be added to the model to visualize the nature of the signals in section of the model. Compared to real number modeling of such a system in Hardware Description Languages(HDL) such as System Verilog or Verilog AMS or VHDL is technically possible, but these models may not be fast to execute as

Simulink. Moreover, Simulink has the advantage of industry standard models and toolboxes in its arsenal.

The simulation of the model starts with the dwell time and the chip rate calculations. The sequences are generated and stored as mat file which are shifted out for every clock. The ADC outputs are saved to database which are postprocessed using Matlab.

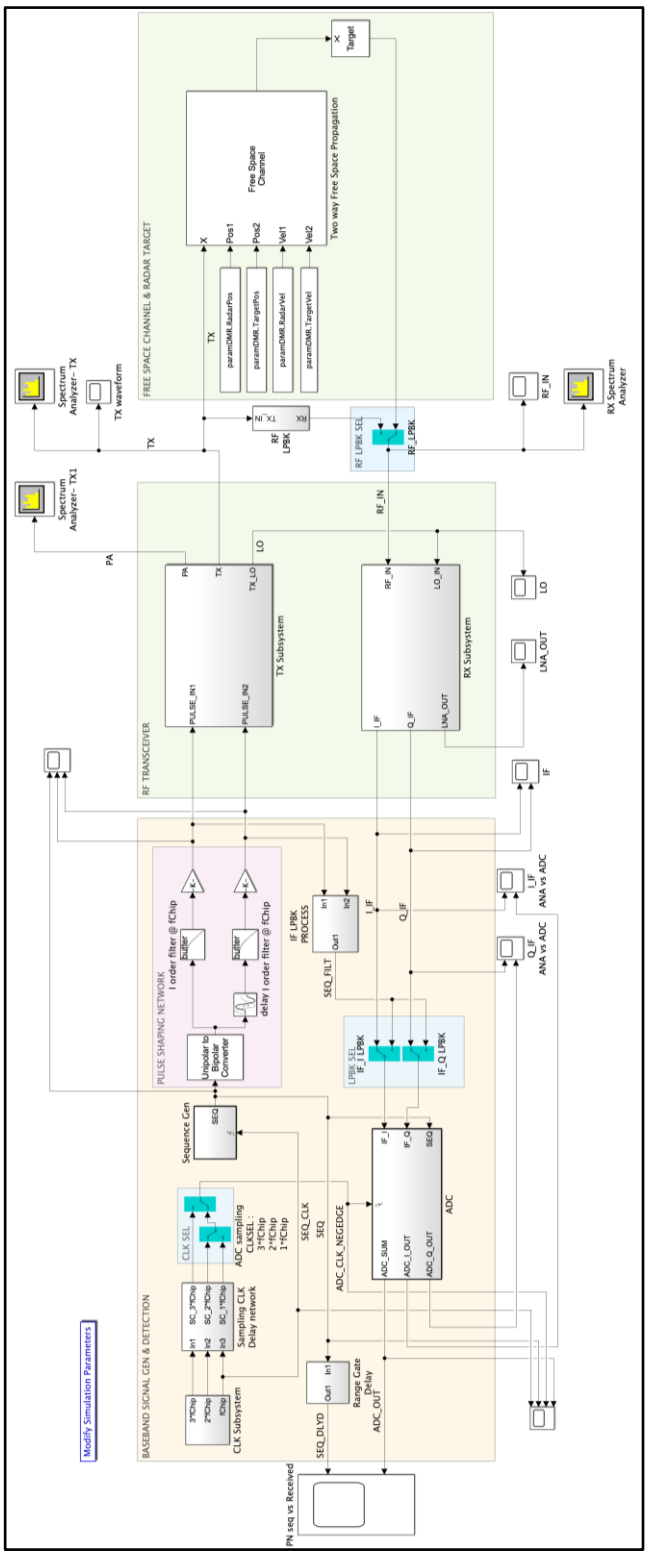

Figure 30: Simulink Model for DMR Transceiver

3.6.2 Equivalent Baseband Model

Though the passband model is useful, DMR requires long transmission of sequences – for a total of (Tc.Lc.M.N) samples of ADC data for a dwell time of 10 milliseconds. Such long sequences are not time efficient with passband models as the minimum time step of the model is governed by the Maximum sampling frequency of the RF carrier clock model. This is usually 5-10 times the carrier frequency and the time step are extremely small.

SimRF blocks also support an equivalent baseband approach for simulating RF systems quicker. Equivalent baseband simulations capture the non-linear RF module's effect on the baseband signal and simulate at the sampling rate required for the baseband models. The RF blockset blocks and the Free space channel comply with this scheme and are very fast to run simulations for the entire dwell time. The Equivalent Baseband models use the same model with a different RF configuration for the TX and RX models.

3.7 Matlab Model for PMCW transceiver

Although equivalent passband model of DMR built in Simulink can simulate faster, it still is not fast enough to simulate an entire frame of dwell time. Moreover, DMR needs MIMO to improve SNR and with Range domain MIMO, the number of samples is increased. Moreover, matlab processes data as multi-dimensional arrays in parallel. To quicken the system model simulation, a matlab model of DMR is also built to simulate the entire system including the signal processing using an equivalent baseband modeling approach. An initial model for the system was available with NXP and changes to this matlab model were based on the Simulink models built so far.

The matlab model includes a sub-modules of waveform generation, transmission, signal attenuation and phase shift based on the target's position and velocity, reception with a finite noise figure in the receiver, and with the same cyclic pipelined ADC to convert it to the discrete level representation. The digital data is then processed using the correlator, accumulator, FFT to recover the radar target position and velocity. The model's modeling approach are detailed in the following sub sections.

3.7.1 Transmitter Model

The matlab model for the transmitter consists of overlapping sequence of length L_C contiguously required for the dwell time(M.N). For every target, the radar range equation is used to estimate the power received at the receiver. The time delay due to reflection off a target at a finite distance is modeled by inserting zeros to the signal vector. After the power reduction due to target, a phase change is also modeled based on the wavelength of the carrier and the distance, and the signals are now represented by complex numbers to show the magnitude and phase present at the receiving antenna's end.

3.7.2 Receiver Front End

The receiver is modeled as one amplifier stage with an input referred system noise figure. For now, only the thermal noise added by the receiver over its noise equivalent bandwidth is considered. The baseband signal is fed to the same cyclic RSD ADC model as used in the Simulink models. The output complex discretized data of the In-phase and Quadrature ADCs are now ready for signal processing.

3.7.3 Signal Processing

Signal processing of radar begins with the matched filtering of the received signal. In DMR, this is accomplished with a correlator. Multiple methods of correlation are in practice – Logic gates, FFT or circular correlator. Though [17] suggests a simple

correlator based on logic gates, this model uses a circular correlator for matched filtering. Circular correlators can be an effective solution for periodic sequences and can be realized with low cost and die area with one multiplier and adder circuit [41].

Circular correlation in DMR can be implemented by shifting the ADC data into a 2D shift register of size Lc rows x M.N columns. Sequences used to transmit can be retrieved from the memory of length (1xLc). Circular shifting of this sequence is done to mimic the 1 chip delay per range gate. The resultant shift register contains a 2D array of size (LcxLc).

3.7.4 Range Processing

Range processing for the radar is performed using correlation of the sequence with the delayed version of the received signal. Correlation of two unipolar binary signals is represented as [41]

$$R(k) = \sum_{n=1}^{Lc} S(n) \oplus RX(n+k)$$

This correlation operation is only valid for the one range gate. To extend it to all range gates of the sequence (Lc) including the integration over Lc, matrix multiplication is performed. The resulting value is the value of lag for every circular shifted to the received waveform.

The resulting matrix is the matched filter output of the system. The processing gain added due to this operation is

$$G_{corr} = 10log_{10}(L_C)$$

As shown in the dwell time calculations, the sequence is repeated for an additional M times for the results to be accumulated. By reshaping the array and adding over M accumulations for every range gate, the signal adds coherently, and the noise adds as random and thereby increasing the signal to noise ration as:

$$G_{acc} = 10\,log_{10}(M)$$

For SISO, the resulting number of data points is a 2D matrix of L_C range gates' N points. A 2D FFT is taken for the entire data to monitor the correlation peak's movement over the range gates. The resulting frequency variation of the correlation peak denotes the movement of the target. The resolution of the FFT bin denotes the minimum and the maximum frequency that is detectable using the set system parameters. The rate of samples to the FFT are given by

$$F_{s-FFT} = L_c\,M\,T_c$$

The resolution of the frequency bin of FFT is

$$F_{res-FFT} = \frac{L_c M T_c}{N}$$

3.7.5 MIMO Processing for Range and Velocity

Range domain MIMO is used in this model using extended sequences ($L_C.N_{TX}$) that are Hadamard transformed, delayed and sent over multiple antennas. These sequences are correlated with the sequence L_C. Correlation result for each range gate for each antenna's Rmax is sorted and Inverse Hadamard transform in performed on the results. This result produced in each Lc wide samples are accumulated for each receiver antenna for M occurences and this data is collected for N FFT bins. A 2D FFT is repeated for each virtual antenna data resulting in a 3D complex data. This data is processed for Doppler processing and Target Range detection across all the virtual antenna arrays. To minimize spectral leakage due to FFT, a window is usually applied to the raw data before FFT.

3.7.6 CFAR Detection

Cell Averaging CFAR method determines the presence of the target based on the power level of the clutter. The postprocessing gain of the correlation, accumulation and

FFT filters most of the random signal power and the SNR improves. CA-CFAR is implemented in matlab using the method explained in Section 2.6.8.

3.7.7 DOA Processing

For the FFT bins detected using CFAR, the phases of the successive virtual array's bins are processed using a simple beamforming algorithm to detect the angle of the target. The resulting azimuth data is collated across all the targets and used to display the radar range, velocity and the angle of arrival.

3.7.8 Radar Range, Velocity, Direction display

The result of the correlation and the FFT of the radar data cube is displayed using three different plots.

a. Target Range Display
b. Target Range, Doppler Display
c. Target Doppler Range and Radar angle display

The Target Range display is the result of correlation and accumulation. For smaller targets may look ambiguous as the processing gain is not complete yet.

The Range, velocity display presents the Radar post processing data after FFT and CFAR detection.

The Radar angle display presents the Angle of Arrival for a MIMO radar case. The next chapter shows the simulation results of different system scenarios and the results of the model.

CHAPTER 4

SIMULATIONS, RESULTS AND DISCUSSION

The model for DMR is represented in three forms:

Simulink based Complex passband model

Simulink based Equivalent baseband model

Matlab model (including Signal Processing)

4.1 Transceiver Simulink model – Passband Simulation

Key Top-Level Specifications used for this simulation are listed below:

System Specifications		
Ambiguous Range	37.474	m
Range resolution	0.749	m
Ambiguous Velocity	11.85	m/s
Velocity Resolution	0.185	m/s
System Parameters		
Chip Rate	1.975	GHz
Sequence Family	APAS	
Sequence Length Lc	1000	
Accumulation length M	160	
FFT points N	128	
Dwell Time	10.36	ms
Target Profile		
Target 1 Range	2	m
Target 1 Velocity	0	m/s
Target 1 Angle	0	degree
Simulation parameters		
ADC ENOB	10	
RX System NF	10	dB

Table 4: Key Top-Level Specifications for Passband Model Simulation

The passband simulation is used to understand the effect of pulse shaping network on the transmitted signal spectrum, passband signal characteristics due to non-idealities

and the reflection characteristics of the radar target. The model exactly reproduces the TX signals shown in IMEC's PMCW radar [16]. The random delay due to the target's location and the free space channel propagation is also observed. Changing the distance of the target, the real and imaginary parts of the radar target can be observed using the model.

The model also clearly shows the LNA outputs with a Noise Figure of 10. This Noise figure value is based on a worst-case test chip measurement and the models are simulated for its performance parameters. The outputs of LNA, and the down converted baseband is observed with the model.

The output of the IF amplifiers is sampled at the chip rate and the output of ADC is seen with one data per chip. The following plot shows the transmitted and received signal waveforms and their spectral content. Observe the phase delay is seen as a complex datatype at the receiver.

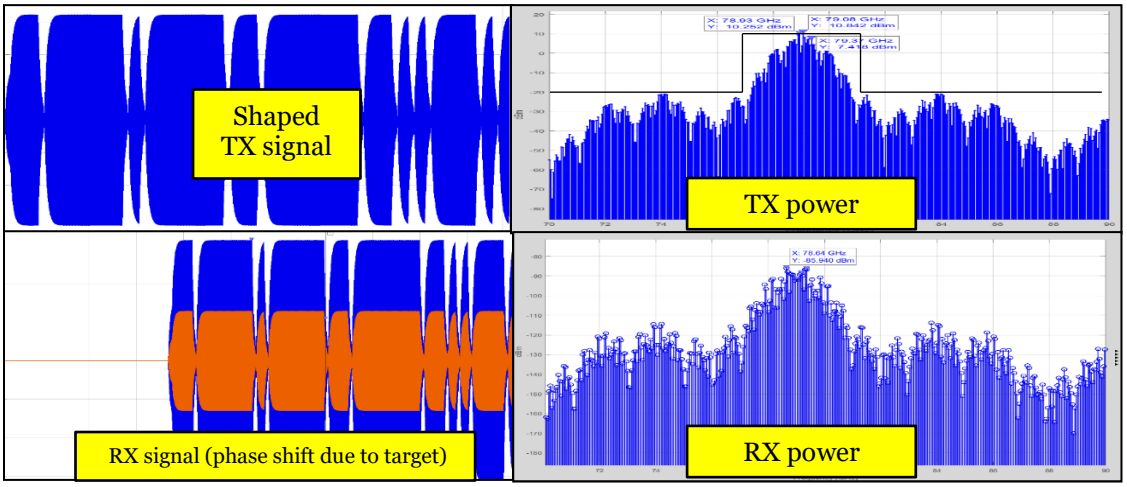

Figure 31: DMR TX and RX Signals and their Spectrum

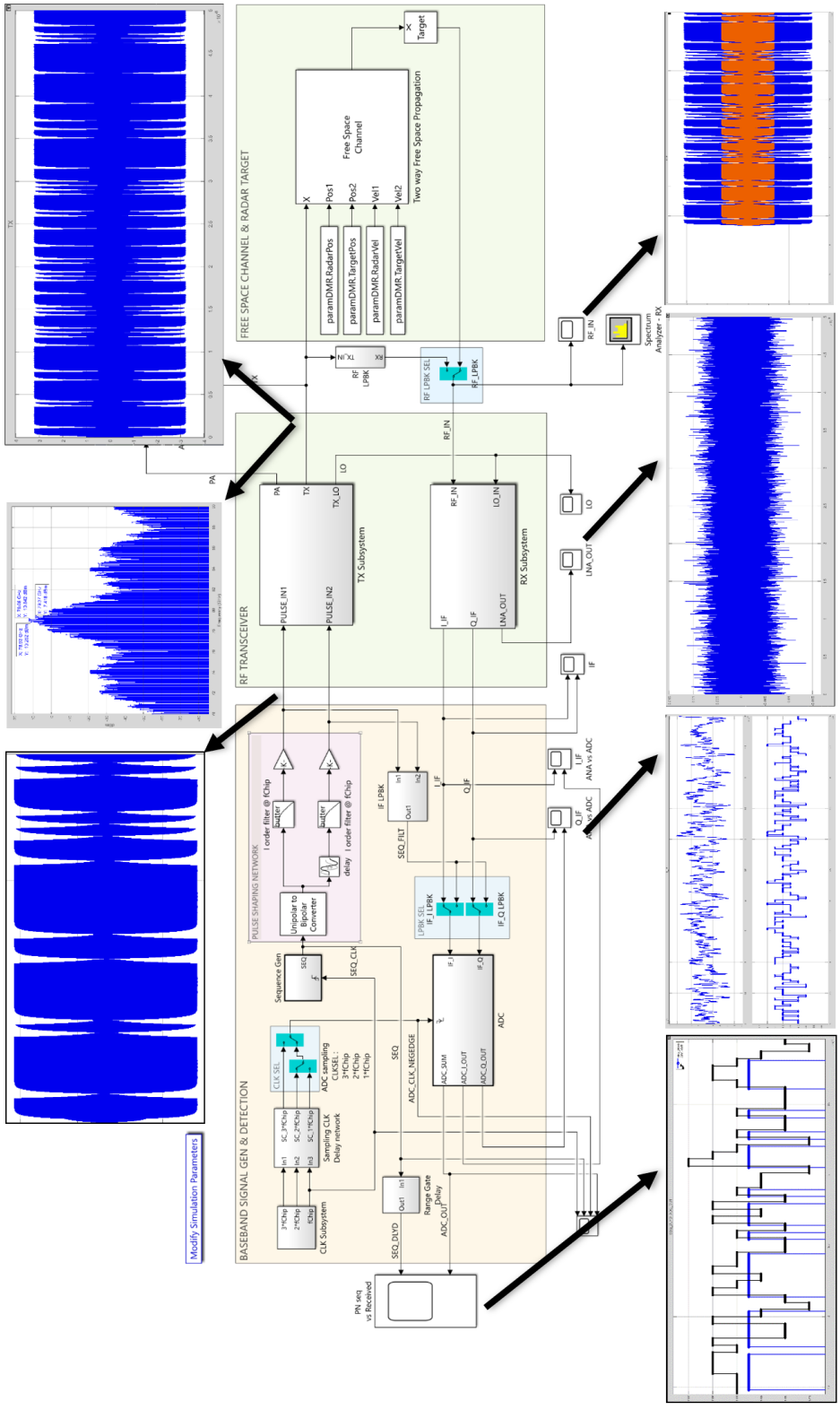

Figure 32: Simulation Results for DMR Passband Model

4.2 Transceiver Simulink Model – Equivalent Baseband Simulation

The same specifications were repeated for the Equivalent Baseband model. As expected, the simulations were much faster and the RF non-ideal characteristics' effect on the baseband is retained in the model.

Simulations were performed for multiple scenarios and data was logged for postprocessing.

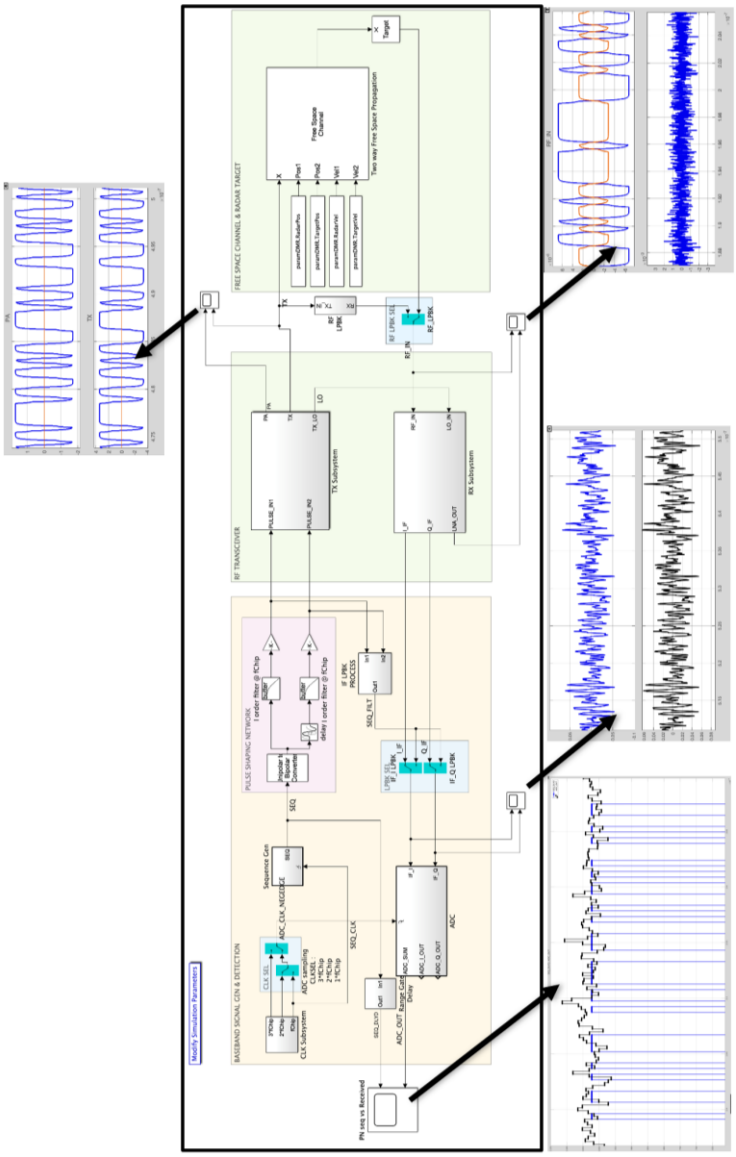

Figure 33: Simulation Results for DMR Equivalent Baseband Model

4.3 Simulations for Target RCS 0 dBsm SISO

Matlab simulations were performed based on the target RCS of 0 dBsm (1 m^2) at a distance of 15m from the radar. The other important specifications are listed below

System Specifications		
Ambiguous Range	37.4741	m
Range resolution	0.749	m
Ambiguous Velocity	11.85	m/s
Velocity Resolution	0.185	m/s
System Parameters		
Chip Rate	2000	
Sequence Family	APAS	
Sequence Length Lc	1000	
Accumulation length M	160	
FFT points N	128	
Dwell Time	10.24	ms
Target Profile		
Target 1 RCS	0	dBsm
Target 1 Range	15	m
Target 1 Velocity	0	m/s
Target 1 Angle	45	degree
Simulation parameters		
Samples	20480000	
ADC ENOB	8	
Post P Gain	73.13	dB

Table 5: Specifications for Scenario #1

For the RCS of 0 dBsm, a very low reflecting target, it can be seen in the following sections that 8 bits ENOB is optimal for the system.

4.3.1 Range Processing

The plot shows the results after correlation over all the range gates. As the target RCS is very low, the range of detection is ambiguous and further post processing is needed.

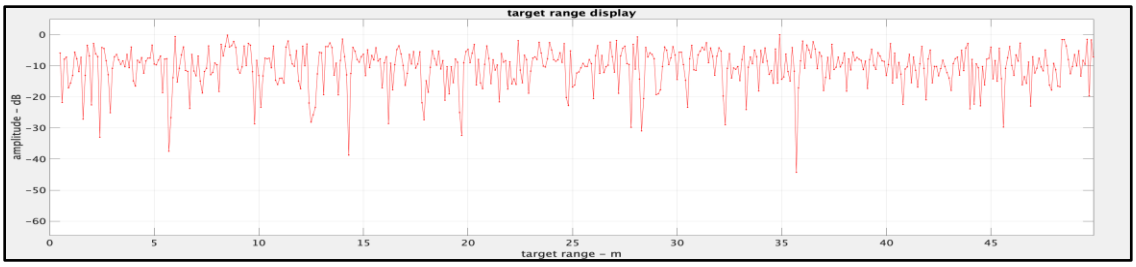

Figure 34: Radar Range profile for Fixed Target SISO 0 dBsm

4.3.2 Range/Doppler Processing

The following plot shows the Range cut of Range-velocity profile. As the post processing gain improves the SNR, the CA-CFAR algorithm detects the presence of the signal among clutter. This is seen in the plot showing the target in the exact range gate.

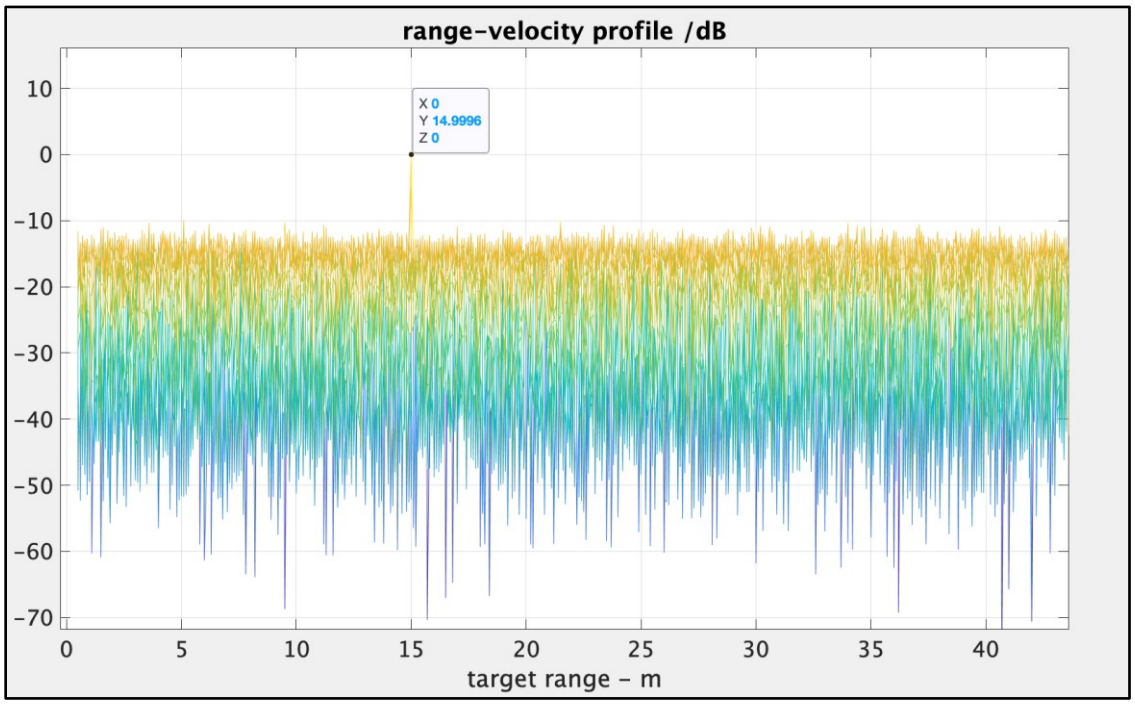

Figure 35: Radar Range Cut in Range-Velocity profile for Fixed Target SISO 0 dBsm

The following plot shows the Range doppler and radar angle of the object. Since this is a SISO scenario, the radar range-angle is not displayed.

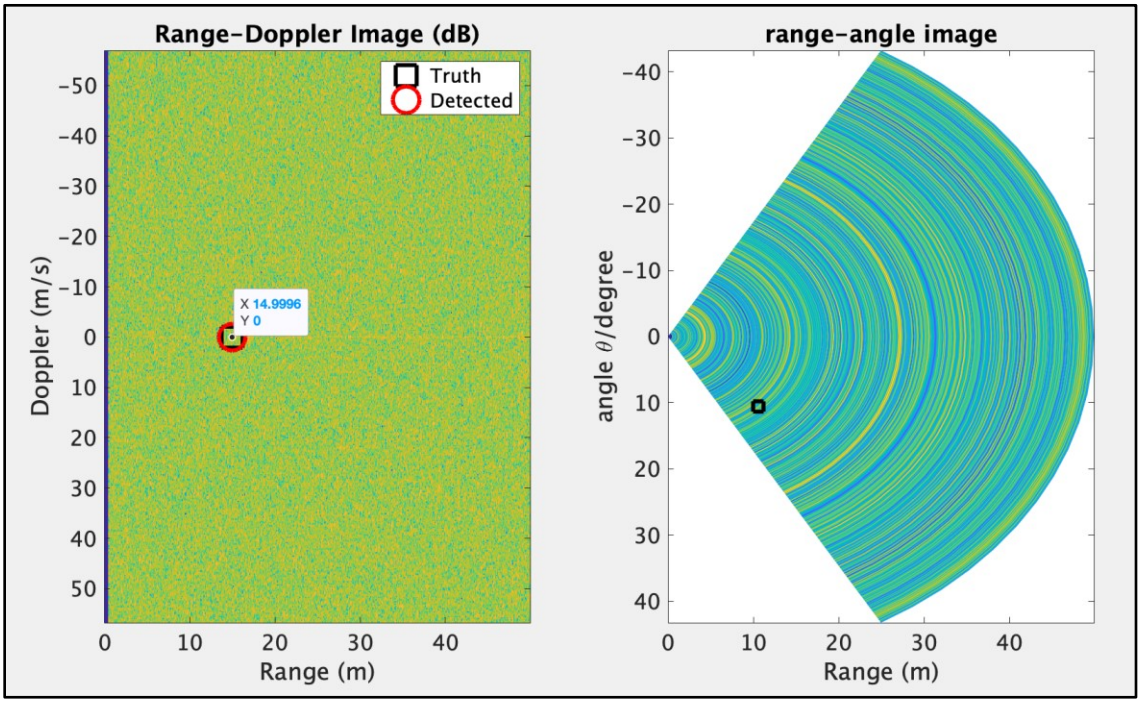

Figure 36: Range-Doppler and Range-Angle for Fixed Target SISO 0 dBsm

4.4 Simulations for Target RCS -8 dBsm SISO

Continuing with the same Range and Range resolution specifications from previous scenario, the target RCS is now reduced to -8 dBsm. This corresponds to a radar cross section of a human in the 76 GHz band [60].

With the lowered RCS and lowered received power, the scenario could not be resolved using an 8 ENOB ADC. After few iterations, with 10 bits of ADC ENOB and in SISO, the simulation passed with other parameters remaining the same.

4.4.1 Range Processing

Since the SNR is lower than the previous scenario (due to lower RCS), the range display using the correlator and accumulator output still remains ambiguous.

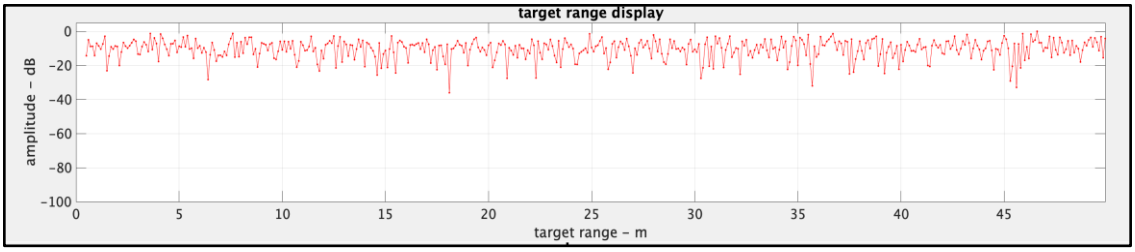

Figure 37: Radar Range profile for Fixed Target SISO -8 dBsm

4.4.2 Range/Doppler Processing

With higher number of ADC bits, the quantization noise added in by the ADC allows more bit toggles in the ADC output that corresponds to the deterministic signal. The range cut profile clearly shows the target at 15m range. The plot also shows the noise floor being higher in this scenario than scenario #1.

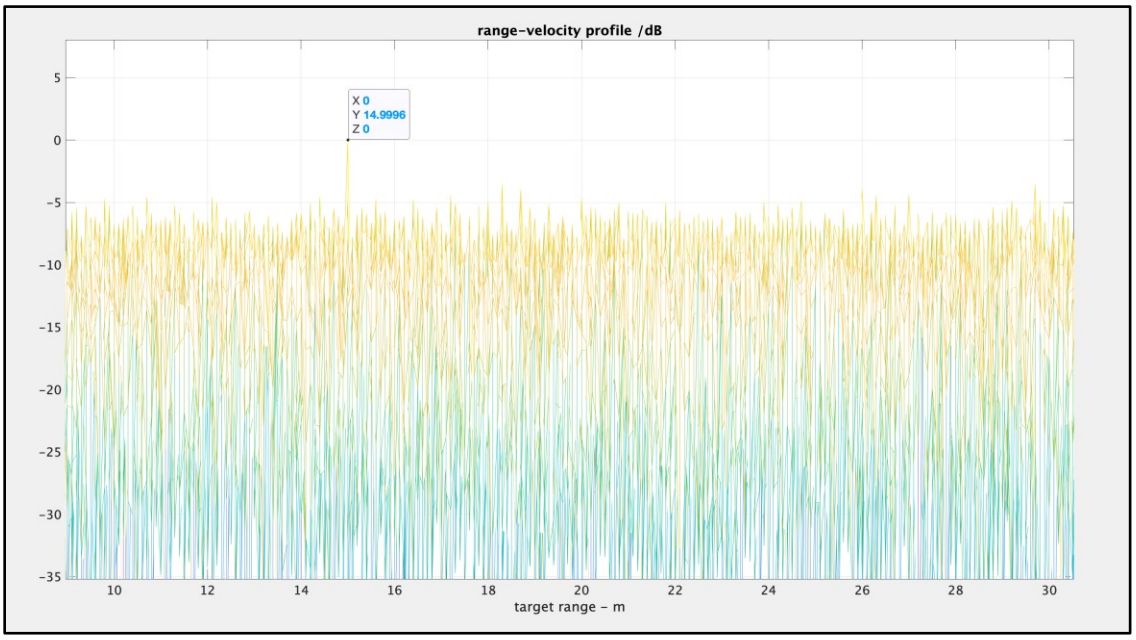

Figure 38: Radar Range Cut in Range-Velocity profile for Fixed Target SISO -8 dBsm

The Range doppler image shows the higher noise floor and locates the object clearly. Notice the object is angle location is still not seen here.

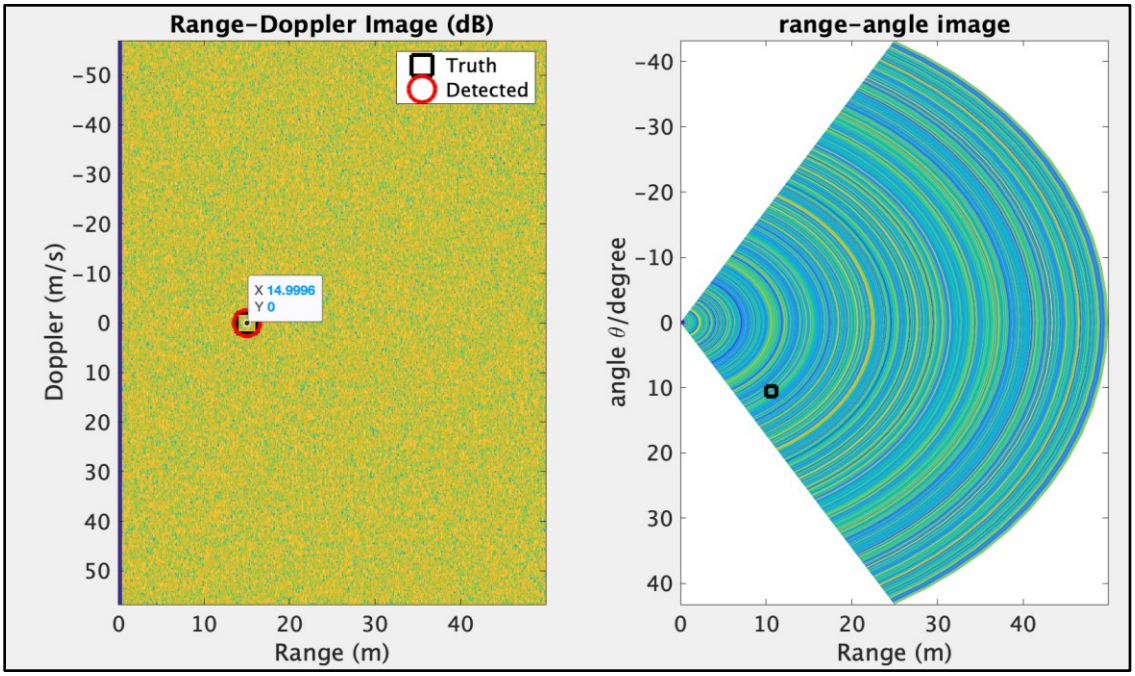

Figure 39: Range-Doppler and Range-Angle for Fixed Target SISO -8 dBsm

4.5 Simulations for Fixed Target RCS 20 dBsm MIMO

With MIMO and beamforming, the Angle of Arrival can be determined. The following table indicates the specifications for this Scenario #3. The MIMO simulations are longer as they use Range domain MIMO. Each receiver channel requires separate ADC and correlator. It is possible to include channel level mismatches in the ADC model also.

System Specifications		
	37.4741	m
Range resolution	0.749	m
Ambiguous Velocity	11.56	m/s
Velocity Resolution	0.18	m/s
System Parameters		
Chip Rate	2000	
Sequence Family	APAS	
Sequence Length Lc	1000	
Accumulation length M	40	
FFT points N	128	
Dwell Time	10.496	ms
NTX	4	
NRX	4	
Target Profile		
Target 1 RCS	20	dBsm
Target 1 Range	30	m
Target 1 Velocity	0	m/s
Target 1 Angle	45	degree
Simulation parameters		
Samples	81920000	
PP Gain	79.1339	dB

Table: Specifications for Scenario #3

4.5.1 Range Processing

The following plot shows the advantages of using MIMO in creating a higher SNR at the receiver. The Range plot indicates the target's location clearly with sufficient SNR. Further post processing increases the SNR even further.

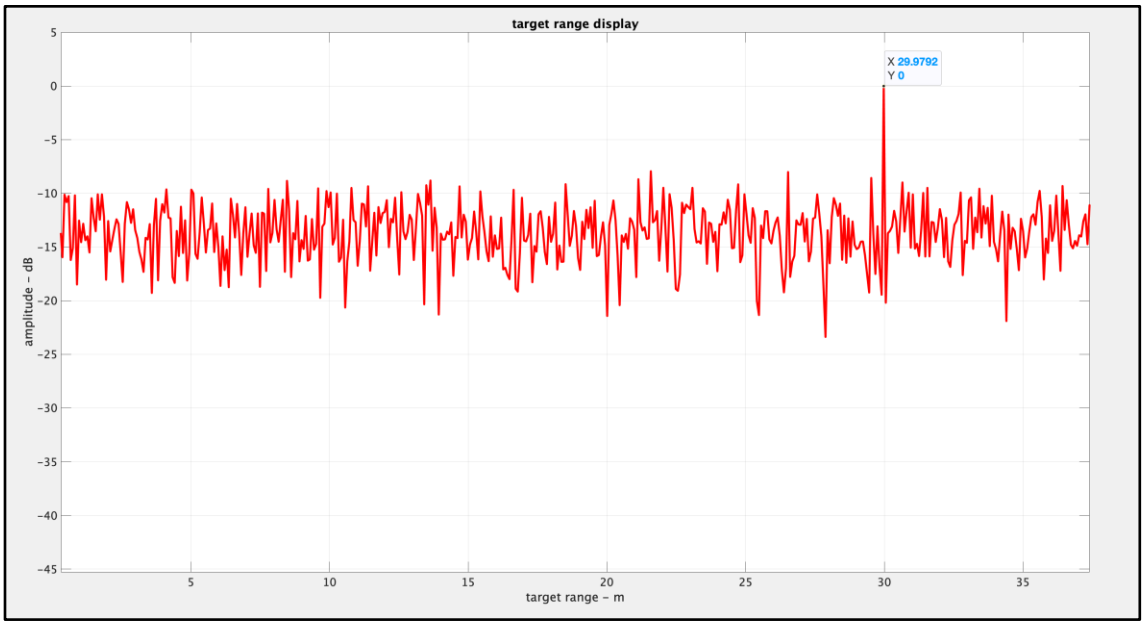

Figure 40: Radar Range profile for Fixed Target MIMO

4.5.2 Range/Doppler Processing

The following figure shows the 3D mesh plot of both range and velocity profile of the target. Since Scenarios #1 and #2 used SISO and stationary targets, the SNR was lower. Hence, only the range cut version of this plot has been shown earlier.

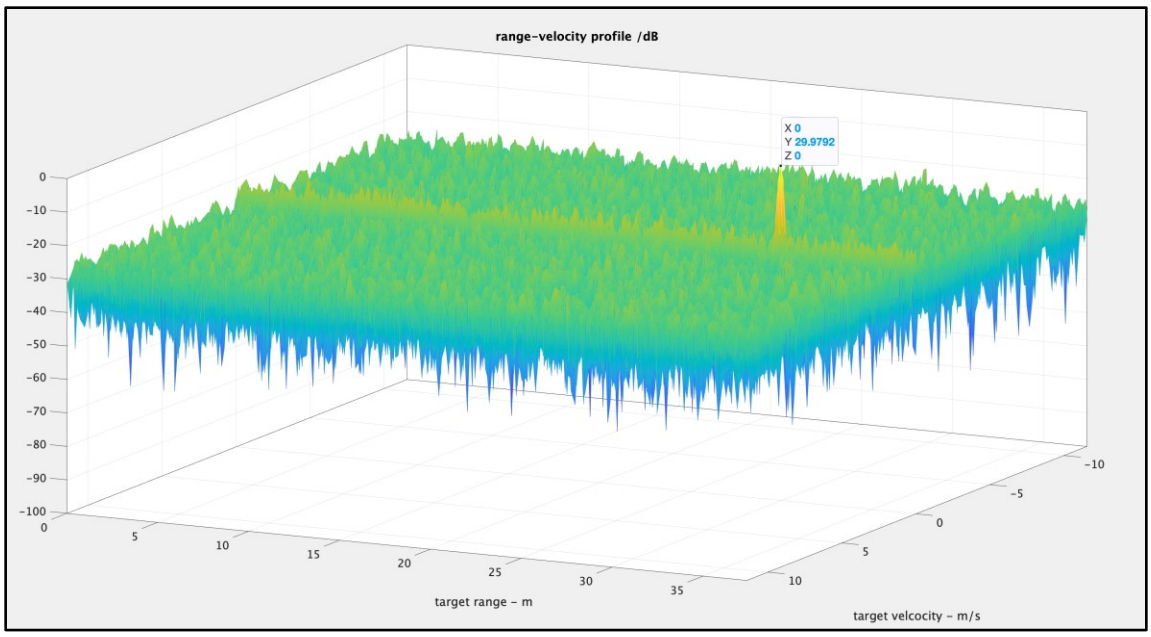

Figure 41: Radar Range-Velocity profile for Fixed Target MIMO

The following plot shows the velocity cut plot of the above mesh plot. As expected, for a stationary target, the velocity peaks at 0 m/s bin of the resulting radar data cube.

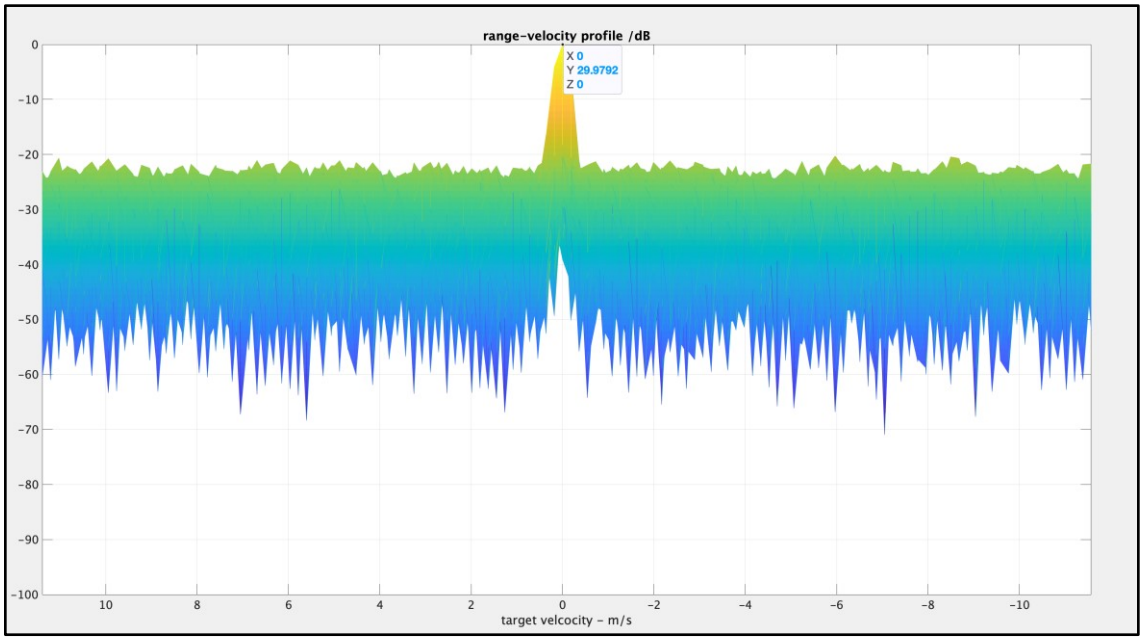

Figure 42: Velocity profile Cut of Fixed Target MIMO

The use of MIMO and beamforming is to determine the angle of arrival of the target to the radar. As shown below, the plot clearly shows the angle of the target that was simulated and estimated. CFAR thresholds for MIMO are higher than SISO due to larger clutter power collected.

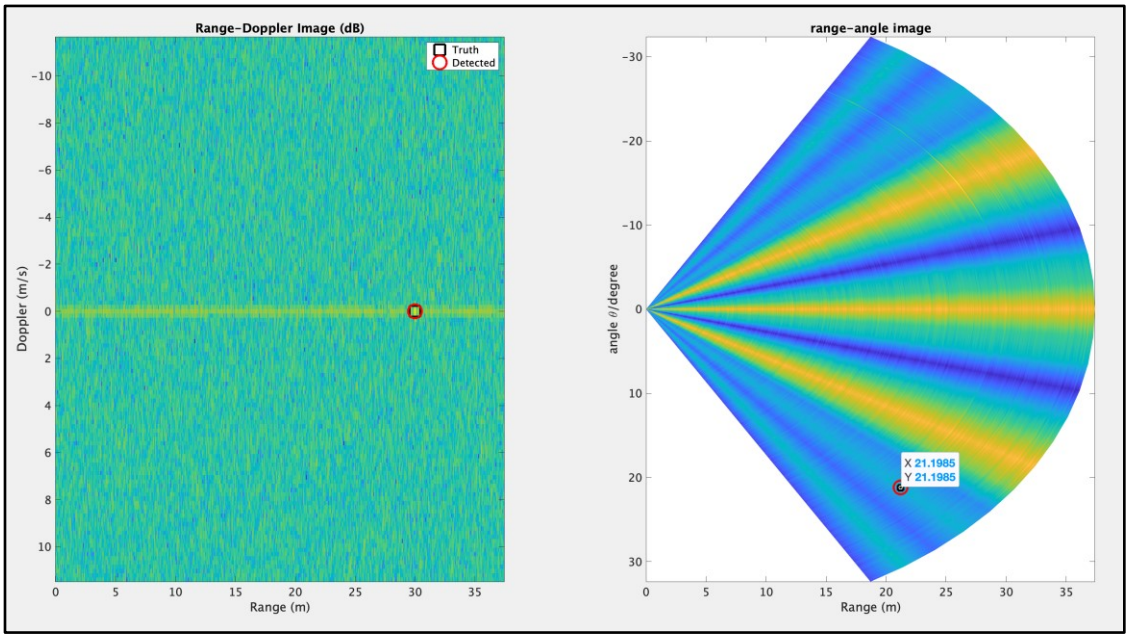

Figure 43: Range-Doppler and Range-Angle for Fixed Target MIMO

4.6 Simulations for Moving Target RCS 20 dBsm MIMO

The simulation of scenario #3 is repeated, but now with a moving target at 10 m/s. The following plots show clearly the Range and the velocity detection by the signal processing routines.

4.6.1 Range processing

The range plot is same as the previous scenario. The model changes the phase of the reflected signal based on the target's velocity. This, however, does not affect the range estimation by correlation and accumulation.

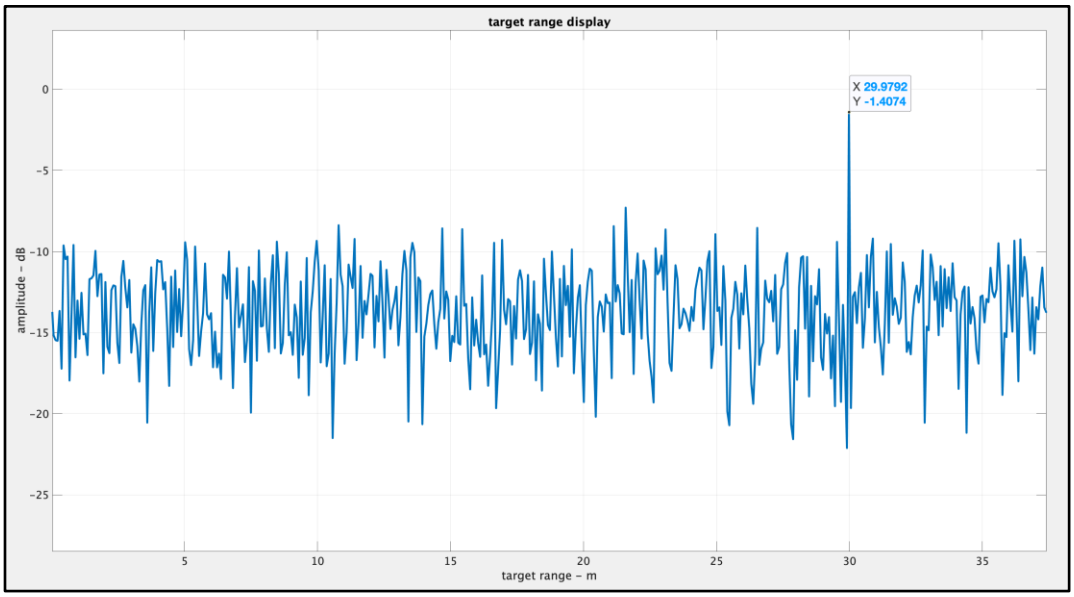

Figure 44: Radar Range profile for Moving Target MIMO

The 3D mesh plot clearly shows the target range and velocity. The velocity component is not exactly 10 m/s due to windowing. The results indicate some more work is needed to select the windowing function for the 2D-FFT.

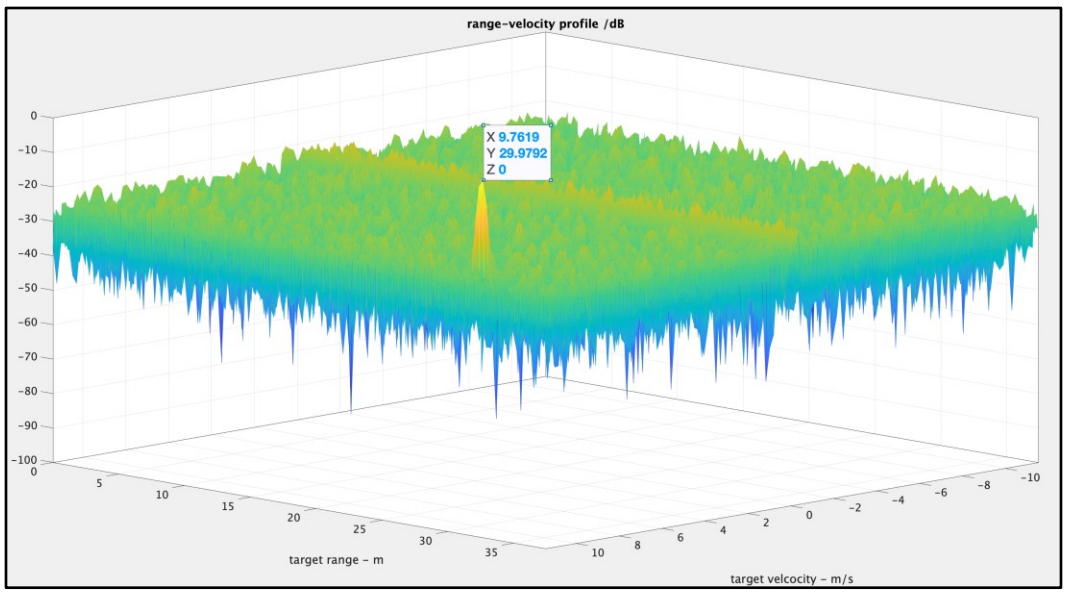

Figure 44: Radar Range-Velocity profile for Moving Target MIMO

4.6.2 Range/Doppler processing

The following plots show the Radar angle and velocity cut profile of the radar-velocity profile. As seen below, the velocity values of the target show up in the target-velocity cut of the range-velocity profile.

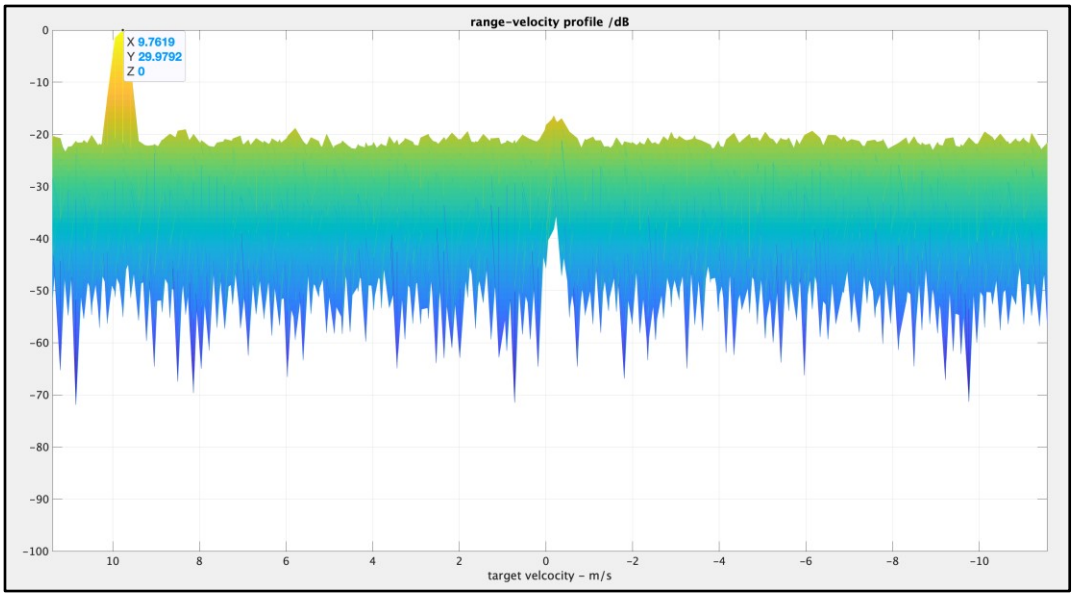

Figure 45: Velocity profile Cut of Moving Target MIMO

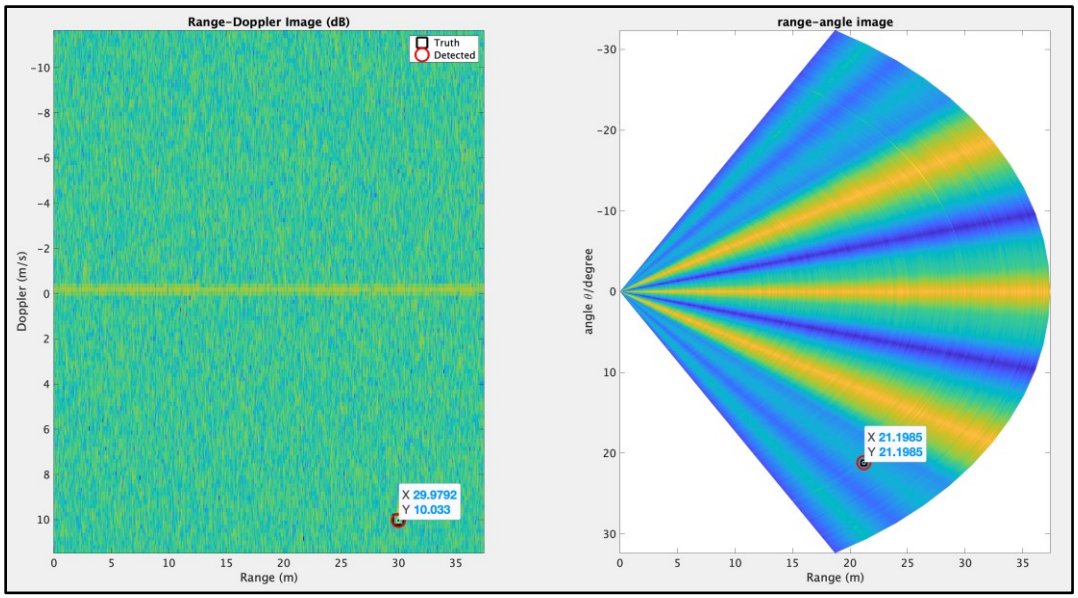

Figure 46: Range-Doppler and Range-Angle for Moving Target MIMO

4.7 Conclusion

System Level Models created for DMR clearly shows the effectiveness of system modeling to understand the behavior that can help make early and avoid expensive design changes. Three different modeling approaches were analyzed and presented. The Simulink models are intuitive to build and the transient behavior every part of the system can be probed and verified. Equivalent baseband simulations can be used to simulate the Simulink models quicker and log data for postprocessing using different signal processing routines for optimized hardware implementation.

The Scenarios discussed above are the select few system usecases that were simulated. These test cases were more targeted towards the MRR and SRR where the RF bandwidth is the widest and the range resolution were the highest.

The simulations indicate many aspects of the system design that can be modified to suit different scenarios to arrive at a suitable design parameter for the radar range and resolution for the end application intended.

CHAPTER 5

FUTURE WORK

This system model can be extended to include the multi path reflection and the interference from other PMCW/FMCW radars to assess the performance. Though there are many advantages for PMCW radars, Overdest's work [40] shows that PMCW radars are affected by interference as much as FMCW radars. Though a lot of the work is done over baseband, it would be fitting to extend this model and simulate for worst possible interference scenarios. Other methods of CFAR detection and MIMO can be introduced to the signal processing routines.

Few other modifications to spread-spectrum based radars are also possible as reported in [39] that uses a Gaussian Minimal Shift Keying of a Quadrature Phase shift keying (QPSK) based radar system. Though a higher data rate is now possible, the system yet uses a 2 Gsps ADC rate. This model can be extended to model GMSK based radar and assess its performance.

REFERENCES

[1] Denny, M. (2007). Blip, Ping, and Buzz: Making Sense of Radar and Sonar. Baltimore: Johns Hopkins University Press.

[2] IEEE Standard for Radar Definitions," in *IEEE Std 686-2017 (Revision of IEEE Std 686-2008)*, vol., no., pp.1-54, 13 Sept. 2017. https://ieeexplore.ieee.org/servlet/opac?punumber=8048477

[3] Wehner, D. (1995). High-resolution radar (2nd ed., Artech House radar library). Boston: Artech House.

[4] Skolnik, & Skolnik, Merrill I. (2008). Radar handbook (3rd ed.). New York: McGraw-Hill.

[5] Razavi, B. (1998). RF microelectronics (Prentice Hall communications engineering and emerging technologies series). Upper Saddle River, NJ: Prentice Hall.

[6] Kevin McClaning. (2012). Wireless Receiver Design for Digital Communications. The Institution of Engineering and Technology.

[7] Meikle, H. (2001). Modern radar systems (Artech House radar library). Boston ; London: Artech House.

[8] Levanon, Nadav, & Mozeson, Eli. (2004). Radar Signals. Hoboken, NJ, USA: John Wiley & Sons.

[9] Mahafza, B. (2000). Radar systems analysis and design using Matlab. Boca Raton: Chapman & Hall/CRC.

[10] Handbook of ultra-wideband short-range sensing; theory, sensors, applications. (2013). Reference and Research Book News, 28(1), Reference and Research Book News, Vol.28(1).

[11] J. Hasch, E. Topak, R. Schnabel, T. Zwick, R. Weigel, and C. Waldschmidt, "Millimeter-wave technology for automotive radar sensors in the 77 GHz frequency band," *IEEE Trans. Microwave Theory Tech.*, vol. 60, no. 3, pp. 845–860, Mar. 2012.

[12] H. H. Meinel, "Evolving automotive radar: From the very beginnings into the future," in *Proc. European Conf. Antennas and Propagation, Hague, The Netherlands, 2014*, pp. 3107–3114.

[13] S. M. Patole, M. Torlak, D. Wang and M. Ali, "Automotive radars: A review of signal processing techniques," in *IEEE Signal Processing Magazine*, vol. 34, no. 2, pp. 22-35, March 2017.

[14] H. J. Ng, R. Feger and A. Stelzer, "A Fully-Integrated 77-GHz UWB Pseudo-Random Noise Radar Transceiver With a Programmable Sequence Generator in SiGe Technology," in *IEEE Transactions on Circuits and Systems I: Regular Papers*, vol. 61, no. 8, pp. 2444-2455, Aug. 2014.

[15] H. J. Ng, R. Feger and A. Stelzer, "A fully-integrated 77-GHz pseudo-random noise coded Doppler radar sensor with programmable sequence generators in SiGe technology," *2014 IEEE MTT-S International Microwave Symposium (IMS2014), Tampa, FL, 2014*, pp. 1-4.

[16] V. Giannini *et al.*, "A 79 GHz Phase-Modulated 4 GHz-BW CW Radar Transmitter in 28 nm CMOS," in *IEEE Journal of Solid-State Circuits*, vol. 49, no. 12, pp. 2925-2937, Dec. 2014

[17] D. Guermandi *et al.*, "A 79-GHz 2x2 MIMO PMCW Radar SoC in 28-nm CMOS," in *IEEE Journal of Solid-State Circuits*, vol. 52, no. 10, pp. 2613-2626, Oct. 2017.

[18] Faus García, Ó. (2015). Signal Processing for mmWave MIMO Radar (Dissertation). Retrieved from http://urn.kb.se/resolve?urn=urn:nbn:se:hig:diva-19866

[19] M. e. a. Kunert, “Mosarim - Project Final Report,” report, 2012.

[20] Bourdoux, K. Parashar and M. Bauduin, "Phenomenology of mutual interference of FMCW and PMCW automotive radars," *2017 IEEE Radar Conference (RadarConf), Seattle, WA, 2017*, pp. 1709-1714

[21] H. P. Beise, T. Stifter and U. Schröder, "Virtual interference study for FMCW and PMCW radar," *2018 11th German Microwave Conference (GeMiC), Freiburg, Germany, 2018*, pp. 351-354.

[22] C. Ma, T. S. Yeo, Q. Guo, C. S. Tan, P. Wei and G. Xu, "Zero Correlation Zone Codes and Extended Zero Correlation Zone Codes for MIMO radar signal separation*," IEEE 10th International Conference on Signal Processing Proceedings, Beijing, 2010*, pp. 2345-2348

[23] A. G. Stove, "Linear FMCW radar techniques," *in IEE Proceedings F - Radar and Signal Processing, vol. 139, no. 5*, pp. 343-350, Oct. 1992.

[24] B. P. Ginsburg et al., "A multimode 76-to-81GHz automotive radar transceiver with autonomous monitoring," *2018 IEEE International Solid - State Circuits Conference - (ISSCC), San Francisco, CA, 2018*, pp. 158-160.

[25] Radar Services in the 76-81 GHz Band, Report and Order – ET Docket No. 15-26, https://docs.fcc.gov/public/attachments/DOC-345476A1.pdf retrieved on June 25, 2019

[26] N. Levanon and B. Getz, “Comparison between linear FM and phasecoded CW radars,” *in Radar, Sonar and Navigation, IEE Proceedings, vol. 141, no. 4. IET, 1994*, pp. 230–240

[27] W. Van Thillo, V. Giannini, D. Guermandi, S. Brebels and A. Bourdoux, "Impact of ADC clipping and quantization on phase-modulated 79 GHz CMOS radar," *2014 11th European Radar Conference, Rome, 2014*, pp. 285-288.

[28] K. Ramasubramanian, “Using a complex-baseband architecture in FMCW radar systems.” (Application Report No. spyy007). Retrieved from Texas Instruments website: http://www.ti.com/lit/wp/spyy007/spyy007.pdf

[29] A. M. D. Turkmani and U. S. Goni, "Performance evaluation of maximal-length, Gold and Kasami codes as spreading sequences in CDMA systems," *Proceedings of 2nd IEEE International Conference on Universal Personal Communications, Ottawa, Ontario, Canada, 1993*, pp. 970-974 vol.2

[30] J. Wolfmann, "Almost perfect autocorrelation sequences*," in IEEE Transactions on Information Theory, vol. 38, no. 4,* pp. 1412-1418, July 1992.

[31] W. Van Thillo, P. Gioffré, V. Giannini, D. Guermandi, S. Brebels and A. Bourdoux, "Almost perfect auto-correlation sequences for binary phase-modulated continuous wave radar," *2013 European Microwave Conference,* Nuremberg, 2013, pp. 1803-1806.

[32] M. Wang, C. H. Chen and S. Radhakrishnan, "Low-Power 4-b 2.5-GSPS Pipelined Flash Analog-to-Digital Converter in 130-nm CMOS," *in IEEE Transactions on Instrumentation and Measurement, vol. 56, no. 3, pp. 1064-1073*, June 2007.

[33] D. Garrity and P. Rakers, "A 10 bit, 2Ms/s, 15 mW BiCMOS cyclic RSD A/D converter," *Proceedings of the 1996 Bipolar/BICMOS Circuits and Technology Meeting,* Minneapolis, MN, USA, 1996, pp. 192-195.

[34] E. Bilhan, P. C. Estrada-Gutierrez, A. Y. Valero-Lopez and F. Maloberti, "Behavioral model of pipeline ADC by using SIMULINK(R)," *2001 Southwest Symposium on Mixed-Signal Design (Cat. No.01EX475),* Austin, TX, USA, 2001, pp. 147-151

[35] L. Dai and X. Liu, "Behavioral Model Based on SIMULINK for 14-bit 200MS/s Pipelined ADC," *2012 International Conference on Control Engineering and Communication Technology,* Liaoning, 2012, pp. 79-82.

[36] Mahafza, B., & Elsherbeni, A. (2004). Matlab simulations for radar systems design. Boca Raton, Fla. ; London: Chapman & Hall/CRC.

[37] M. A. Belkerdid and T. Mears, "Sinusoidal SBPSK Modulation Waveform for UHF SATCOM Channels with Improved Adjacent Channel Emissions," *MILCOM 2007 - IEEE Military Communications Conference, Orlando, FL, USA, 2007*, pp. 1-7.

[38] S. Trotta, B. Dehlink, H. Knapp, K. Aufinger, T. F. Meister, J. Bock, W. Simburger, and A. L. Scholtz, “SiGe Circuits for Spread Spectrum Automotive Radar,” *in 2007 IEEE International Conference on Ultra-Wideband, 2007*, pp. 523–528.

[39] V. Giannini et al., "9.2 A 192-Virtual-Receiver 77/79GHz GMSK Code-Domain MIMO Radar System-on-Chip," *2019 IEEE International Solid- State Circuits Conference - (ISSCC),* San Francisco, CA, USA, 2019, pp. 164-166.

[40] Overdevest, Jeroen “Interference in 79 GHz Phase-Coded Automotive Radar”, Thesis report, Delft University of Technology. http://resolver.tudelft.nl/uuid:a22d5686-0d83-402b-94cc-4b49c2a63853

[41] S. Šajić, N. Maletić, M. Šunjevarić and B. Todorović, "Low-cost digital correlator for frequency hopping radio," *2011 18th International Conference on Systems, Signals and Image Processing,* Sarajevo, 2011, pp. 1-4.

[42] M. Uchida, Y. Kagawa and A. Okuno, "A vehicle-to-vehicle communication and ranging system based on spread spectrum technique-SS communication radar," Proceedings of VNIS'94 - *1994 Vehicle Navigation and Information Systems Conference,* Yokohama, Japan, 1994, pp. 169-174.

[43] Y. Ji-yang, P. Bo, H. Dan, S. Xiao-hu and W. Lu-yuan, "On-board spread spectrum signal correlation detection design based on FFT," *2016 IEEE 13th International Conference on Signal Processing (ICSP),* Chengdu, 2016, pp. 1180-1185.

[44] Y. Kim, "Identification of FMCW radar in mutual interference environments using frequency ramp modulation," *2016 10th European Conference on Antennas and Propagation (EuCAP),* Davos, 2016, pp. 1-3.

[45] J. Muñoz-Ferreras, Z. Peng, C. Li and R. Gómez-García, "Effects and mitigation of interference tones on coherent FMCW short-range radars," *2016 IEEE MTT-S International Wireless Symposium (IWS),* Shanghai, 2016, pp. 1-4.

[46] T. Nozawa et al., "An anti-collision automotive FMCW radar using time-domain interference detection and suppression*," International Conference on Radar Systems (Radar 2017),* Belfast, 2017, pp. 1-5.

[47] V. Venkatasubramanian and H. Leung, "A robust chaos radar for collision detection and vehicular ranging in intelligent transportation systems," *Proceedings. The 7th International IEEE Conference on Intelligent Transportation Systems (IEEE Cat. No.04TH8749)*, 2004, pp. 548-552.

[48] V. Venkatasubramanian, Peiguo Liu and H. Leung, "Chaos based UWB imaging radar for homeland security," *IEEE Conference on Cybernetics and Intelligent Systems, 2004.*, 2004, pp. 351-355 vol.1.

[49] F. V. Schultz, R. C. Burgener and S. King, "Measurement of the Radar Cross Section of a Man," in *Proceedings of the IRE*, vol. 46, no. 2, pp. 476-481, Feb. 1958.

[50] J. D. Woll, "Monopulse Doppler radar for vehicle applications," *Proceedings of the Intelligent Vehicles '95. Symposium*, Detroit, MI, USA, 1995, pp. 42-47.

[51] L. H. Eriksson and B. -. As, "Automotive radar for adaptive cruise control and collision warning/avoidance," *Radar 97* (Conf. Publ. No. 449), Edinburgh, UK, 1997, pp. 16-20.

[52] C. Eckersten and B. -. As, "A high performance automotive radar for adaptive cruise control and collision warning/avoidance," *Proceedings of Conference on Intelligent Transportation Systems*, Boston, MA, USA, 1997, pp. 446-451.

[53] Electronic Warfare and Radar Systems Engineering Handbook, by Avionics Department, OCTOBER 2013, NAVAL AIR WARFARE CENTER WEAPONS DIVISION POINT MUGU, CA 93042

[54] G. Palubinskas and H. Runge, "Radar Signatures of a Passenger Car," in *IEEE Geoscience and Remote Sensing Letters*, vol. 4, no. 4, pp. 644-648, Oct. 2007. doi: 10.1109/LGRS.2007.903074

[55] N. A. M. Daud, N. E. A. Rashid, K. A. Othman and N. Ahmad, "Analysis on Radar Cross Section of different target specifications for Forward Scatter Radar (FSR)," *2014 Fourth International Conference on Digital Information and Communication Technology and its Applications (DICTAP)*, Bangkok, 2014, pp. 353-356.

[56] Z. Slavik, A. Viehl, T. Greiner, O. Bringmann and W. Rosenstiel, "Compressive sensing-based noise radar for automotive applications," *2016 12th IEEE International Symposium on Electronics and Telecommunications (ISETC)*, Timisoara, 2016, pp. 17-20.

[57] Z. Liu, D. Liu, J. Zhang and J. Liu, "Modulation and demodulation circuits of MIMO radar based on qpsk," *2017 Sixth Asia-Pacific Conference on Antennas and Propagation (APCAP)*, Xi'an, 2017, pp. 1-3.

[58] N. Levanon, "CW alternatives to the coherent pulse train-signals and processors," in *IEEE Transactions on Aerospace and Electronic Systems*, vol. 29, no. 1, pp. 250-254, Jan. 1993.

[59] J. Li and P. Stoica, MIMO Radar Signal Processing. John Wiley & Sons, 2008.

[60] N. Yamada, Y. Tanaka and K. Nishikawa, "Radar cross section for pedestrian in 76GHz band," 2005 European Microwave Conference, Paris, 2005, pp. 4 pp.-1018.

[61] EEE 527: Nyquist Rate Data Converters Course Notes at Arizona State University, Dr Doug Garrity, 2018

[62] N. Levanon, I. Cohen: "Binary frequency shift keying for continuous waveform radar", IEEE Trans on Aerospace and Electronic Systems., Vol. 53 (5), pp. 2462 - 2468, Oct 2017.